University of Kerbala

College of Science

Department of Physics

Finding Some Rate Equations Parameters for Passively Q -Switched Lasers Using Optimization Technology

A Thesis Submitted to the Council of the College of Science- University of Kerbala in Partial Fulfillment of the Requirements for the Master Degree in Science of Physics

Written by

Duaa Sabbar Salman

Supervised by

Dr. Qasim Hassan Ubaid

2025 A. D. **1447 A. H.**

بِسْمِ اللَّهِ الرَّحْمَنِ الرَّحِيمِ

يَرْفَعِ اللَّهُ الَّذِينَ آمَنُوا مِنكُمْ وَالَّذِينَ أُوتُوا الْعِلْمَ دَرَجَاتٍ

صدق الله العلي العظيم

سورة المجادلة- الآية (11)

Supervisor Certificate

We certify that the thesis entitled " **Finding Some Rate Equations Parameters for Passively Q -Switched Lasers Using Optimization Technology"** was prepared under our supervision by (**Duaa Sabbar Salman**) at the Science College / Kerbala University as a partial fulfilment of the requirements for the M.Sc. Degree of Science in Physics.

Signature:

Name: Dr. Qasim Hassan Ubaid

Title: Lecturer

Date 27 / 8 / 2025

Certification of the Head of the Department

In view of the available recommendations, I forward this thesis for debate by the examining committee.

Signature: M. A. AL-KAABI

Name: Dr. Mohammed Abdulhussain AL-Kaabi

Title: Assistant Professor

Head of Physics Department, College of Science, University of Kerbala

Date: 11 / 9 / 2025

Examination Committee Certification

We certify that we have read this thesis, entitled **"Finding Some Rate Equations Parameters for Passively Q -Switched Lasers Using Optimization Technology"** and as an examining committee, examined the student **"Duaa Sabbar Salman"** on its contents and that in our opinion it is adequate for the partial fulfillment of the requirements for the Master Degree of Science in Physics.

Signature
Name: **Dr. Khawla Jameel Tahir**
Title: Professor
Address: University of Kerbala, College of Science, Department of Physics.
Date: 24/8/2025
(Chairman)

Signature
Name**: Dr. Mohammed Abdullah Hameed**
Title: Professor
Address: University of Baghdad, College of Science, Department of Physics.
Date: 2 / 9 / 2025
(Member)

Signature: Azhr.A.R
Name: **Dr. Azhr Abdulzahraa Raheem**
Title: Assist Professor
Address: University of Kerbala, College of Science, Department of Physics.
Date: 24/8/2025
(Member)

Signature:
Name: **Dr. Qasim Hassan Ubaid**
Title: Lecturer
Address: University of Kerbala, College of Science, Department of Physics.
Date: 27/8/2025
(Member & Supervisor)

Signature:
Name: **Dr. Hassan Jameel Jawad AL-Fatlawy**
Title: Professor

Address: **Dean of the College of Science, University of Kerbala**
Date: / /

Dedication

-----To those who, after Allah, have been a source of support and inspiration my dear parents. I dedicate the fruit of my effort in recognition of your kindness and in appreciation of your immense generosity.

-----To my beloved husband, my partner in life and the supporter of my journey, who has never hesitated to offer me care and encouragement. Thank you for standing by my side every step of the way and for believing in my abilities.

-----To my dear children, the flowers of my life and the joy of my days. You are the greatest motivation for me to keep going and giving. I hope this achievement will be a source of pride for you, just as you are for me.

-----To my esteemed professors in the department, who illuminated my path with knowledge and wisdom and did their utmost to guide me toward excellence and creativity. Thank you for every word of wisdom and learning.

Duaa

Acknowledgement

I am truly thankful to my supervisor, Dr. Qasim Hassan Ubaid, for his constant motivation, generous assistance, and for always being available to offer help and advice whenever I needed it.

I would also like to thank all the members of staff at college of Science Physics Department.

List of Contents

List Figures

Abbreviations

Abbreviation	Meaning
TOC	Thermo-Optics Coefficient
MEMS	Micro Electro-Mechanical Systems

NLO	Nonlinear Optical
Abbreviation	**Meaning**
HOS	Hybrid Optical Switching
Q	Quality Factor
AO	Acousto-Optic
Ge	Germanium
TeO2	Paratellurite
CO2	Carbon Dioxide
RF	Radio Frequency
KDP	Potassium Dihydrogen Phosphate
LN, LiNbO3	Lithium Niobate
DC	Direct Current
SA	Saturable Absorber Material
PML	Passive Mode Locking
NPL	Nuclear Pumped Lasers
Cr: LiSAF	Chromium-doped Lithium Strontium Aluminum Fluoride
LOC	Lightning Optical Corporation
OSCs	Organic Solar Cells
LEDs	Light-Emitting Diodes
EDFL	Erbium-Doped Fiber Laser
LDPSSLs	Laser Diode Pumped Solid-State Lasers
SESAM	Semiconductor Saturable Absorber Mirror
LD	Low-Dimensional
2D	Two-Dimensional
1D	One-Dimensional
TIs	Topological Insulators
TMDs	Transition Metal Dichalcogenides
BP	Black Phosphorus
CNTs	Carbon Nanotubes
QDs	Quantum Dots
Cr: YSO	Chromium-Doped Yttrium Orthosilicate
Cr: LiCAF	Chromium-Doped Lithium Calcium Aluminum Fluoride
OCT	Optical Coherence Tomography
GA	Genetic Algorithm
ACA	Ant Colony Algorithm
PSO	Particle Swarm Algorithm
ni	Saturable Absorber Molecules
BLF	Barrier Lyapunov Function

Symbols

Symbol	Description
Q	Quality factor.
E	Pulse energy (J).
ν	Frequency of the laser beam (h).
α_C	Absorption coefficient of unit length(cm).
n_0	Refractive index of the effective medium.
C	Speed of light (m/s).
L	Length of resonator (cm).
T	Duration one cycle time (s).
R_1 R_2	Reflectivity of mirrors.
M	Magnification factor of the round trip.
σ_T	Cross-section of the permeability (cm^2).
$N_1 N_2$	Qualification of levels (1) and (2) respectively.
L_o	Output loss.
R_o	Peak reflectivity.
N_g	The laser population inversion (cm^{-3}).
g	Level degeneracy.
α_{g_0} α_{a_0}	Absorption coefficients of the unexcited laser and absorber centers respectively(cm).
ϕ	Photons density (cm^{-3}).
t_1	Cavity signal pass time(s).
t_c	Cavity photon lifetime(s).
γ	Fractional photon loss for a double pass in the cavity.
α_0	Absorption coefficient of non-excited laser material (cm^{-1}).
σ_g	Cross-section of the amplifying centers(cm).
σ_a	Cross-section of the absorbing centers(cm).
τ_a	The absorber emission life time (sec).
Na	The ground state population of the saturable absorber (cm^{-3}).
N	Photon density inside the laser resonator (cm^{-3}).
N_{ao}	Initial value of Na (cm^{-3}).
N_{th}	Laser threshold population inversion (cm-3).
Rp	Pumping rate (sec^{-1}).
γ_g	Effective decay rate of the upper laser level (sec^{-1}).
Tg	Laser emission life time (sec).
Kg	Active medium coupling coefficient (sec^{-1}).
τ_r	Transit time for one round –trip (s).
A_g	Effective laser beam area on the laser gain medium (cm).

Symbol	Description
σ_{ag}	Saturable absorber ground –state absorption cross (cm^2).
Ka	Saturable absorber coupling coefficient (sec^{-1}).
Aa	Effective laser beam area on the saturable absorber (cm).
γ_c	Cavity decay rate (sec^{-1}).
τ_c	Cavity life time (sec).
α_0	Absorption coefficient per unit length(cm).
l_r	Length of the laser rod (cm).
σg. s. a	Exited state absorption cross-section of saturable absorber (cm^2).

List of Tables

Abstract

This study, aims to find the optimal values of some coefficients of the rate equations for a Cr : LiSAF laser Q-switched by Cr: YSO saturable absorber.

The mathematical model used is based on four first-order nonlinear differential equations that represent the evolution of the temporal behavior of the system components, as follows.

The first equation represents the rate equation for the cavity photon number (n). The second stands for the rate equation for the gain medium with population inversion (N_g). The third serves the rate equation for saturable absorber molecule at the ground state (N_a). The fourth represents the rate equation for saturable absorber molecule at the first excited state (N_{au}). It was solved numerically using Runge – kutta – fehlberge method to determine the characteristics of the laser-generated giant pulse.

After that the optimization technique was utilized to determine the following parameters, the excited state absorption cross-section to the ground state absorption cross-section of the saturable absorber molecules (β), the saturable absorber decay rate (γ_a), photons losses inside the laser cavity(γ_c), using constrained Rosenbrock optimization technique. Where it was found that the value of (β)increases with increasing the number of Cr: YSO molecules number, but values of both Cr: YSO relaxation rate (γ_a) and photons losses rate (γ_c) decrease with increasing number of Cr: YSO saturable absorber molecules number until reaching a certain value, at which point the variation becomes negligible. Optimal solutions were reached with accuracy and balance that achieve the best operating conditions for the laser system. The absolute error ratio between the theoretically calculated and the practically calculated parameters was (0.0299, 0.000009, 0.0000032), respectively.

Chapter One: Introduction

1.1. Introduction

This chapter serves as an introduction to optical switches, providing an overview of their progress over time and some of their applications. Several types of switches are mentioned, such as thermo-optic switches, microelectromechanical switches, liquid crystal switches, and hybrid nonlinear switches. The chapter also presents the objective of this study.

1.2. Optical switches

Switches are a device that uses binary numbers, zero and one, to signify "on" and "off"[1]. Optical switches are essential for enhancing optical communication systems and attaining high data transmission rates in integrated optical circuits [2].The primary advantage of optical switching is its capacity to route optical data impulses without converting them to electrical signals, rendering it independent of data rate and protocol [3]. Optical switching applications are effectively executed in high-speed signal processing using all-optical gates [4], extremely essential for the future of mobile broadband all-optical IP networks [5] and optical cross-connects[6]. Optical crossconnects serve as fundamental components for routing optical communications inside an optical network or system [3].

Optical switches can be classified into several groups (for example):

1.2.1. Thermo-Optic Switches

The Thermo-Optic effect refers to the alteration in the refractive index of a dielectric substance caused by a change in the material's temperature. The thermo-optic effect exists in all materials and is characterized by the Thermo-Optics Coefficient (TOC), defined as dn/dT, where n represents the refractive index of the material at temperature T. The TOC is of considerable importance in several optical

and optoelectronics applications, including the guidance, coupling, and modulation of radiation [7]. The predominant materials employed in the manufacturing of thermo-optical switches are polymers and silica [8]. The most attractive feature of polymer waveguide technology is the simplicity and versatility of waveguide production techniques, along with the accessibility of a diverse array of inexpensive optical polymers that exhibit superior optical, chemical, and mechanical characteristics [7]. Polymer classes are utilized in integrated optics comprise acrylates, polyimides, and olefins (e.g., cyclobutene). The majority exhibits transparency within the wavelength range of 400 to 2000 nm [9]. Yet, they may suffer from high driving power and significant power dissipation [7].

1.2.2. Micro Electro-Mechanical Systems Optical Switches

This switch is a variant of the mechanical switch known as a "optomechanical switch" [6]. Micro electromechanical systems (MEMS) are small devices measuring in the micrometer range. They are typically fabricated from silicon substrates using a manufacturing process. Consequently, several micro electromechanical systems devices may be fabricated on a single silicon substrate. The dimensions of the devices range from micrometers to millimeters. In micro electromechanical systems technology for optical switches, the mirror orientations dictate the switching functionality of the devices. The locations may be altered by adjusting the mirrors [3, 6]. Electrostatic or electromagnetic forces are employed to modify the locations of these mirrors. This signifies that optical signals can go from one location to another by reflecting off mirrors. MEMS optical switches have several advantages, including scalability and insensitivity to wavelength and polarization, making them appealing diverse domains such as research, industry, and telecommunications production [10].

Two prevalent methodologies exist for the implementation of micro electromech-

anical systems optical switches [11]. As shown in the Figure (1-1):

•2D micro electromechanical systems switches

•3D micro electromechanical systems switches

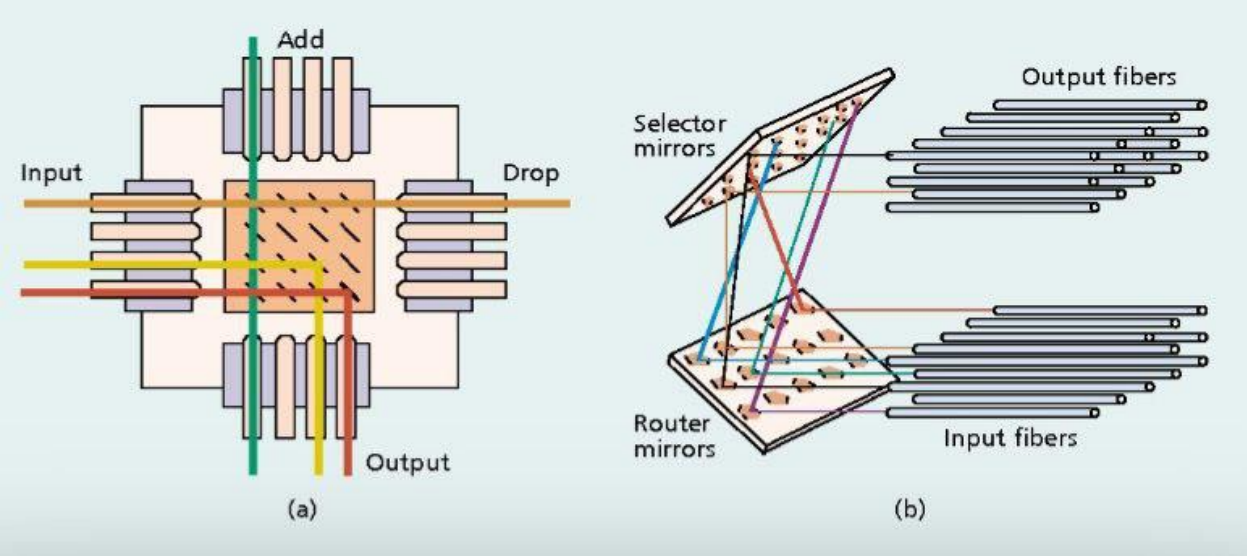

Figure: (1-1) Micro electromechanical systems methodologies for optical crossconnect switching: a)Digital or two-dimensional micro electromechanical systems technology: b) Analog, scanning mirror, or three-dimensional technology [3].

1.2.3. Liquid Crystal Optical Switches

Certain organic compounds have a molecular order that is transitional between crystalline solids and amorphous liquids, contingent upon the ambient temperature. These substances are designated as thermotropic liquid crystals[12]. Liquid-crystal modulators employ polarization manipulation to direct optical signals without the use of movable mechanical components [13]. There are three types of liquid crystal[14]:

- Thermotropic they exhibit mesophases as a function of temperature without the need for solvents, and are widely used in optical switching due to their sensitivity to thermal and electric stimuli.
- Lyotropic they form mesophases based on the concentration of amphiphilic molecules in a solvent, with structural behavior influenced by both temperature and concentration.
- Polymeric They consist of macromolecules that retain liquid crystalline properties, providing enhanced mechanical stability and thermal durability in advanced optical applications.

Liquid-crystal cells need minimal control voltages and currents. Consequently, they utilize less power than optomechanical switches. Liquid-crystal material has little absorption in the infrared spectrum [13].

1.2.4. Nonlinear Optical Switches

Researchers have attempted to manufacture and analyze several molecular Nonlinear Optical switches. This switches differ according on the stimulus employed to induce commutation these stimuli may encompass light irradiation, redox reactions and pH variations [15]. Photochromes, acid ochromes or halochromes, thermochromes, and electrochromes are the terms used to describe chemicals that generate a spectrum change, often of visible color, but not always. Aside from changes in linear optical properties (light absorption and emission), reactivity, and complexation behavior, stimuli can also cause variations in nonlinear optical (NLO) properties such as second-harmonic generation, two-photon absorption, and third-harmonic generation[16]. An optical switch can quickly transmit or reject an optical signal. However, the majority of integrated optical switches developed to date rely on thermo-, magneto-, or electro-optical

phenomena, which restrict applications owing to sluggish reaction times, huge footprints, and manufacturing complexity.

[17]. The need for the development of high-performance nonlinear optical materials is significant due to the rise of photonic technologies in telecommunications, where information is encoded, transmitted, and routed optically [18-20]. The switchable nonlinear optical characteristics can function as readout signals for sensing and data storage [21]. A significant quantity of NLO materials has been created in the past two decades. Optical signaling, as an innovative communication approach, facilitates enhanced network speed and expanded bandwidth [22].

1.2.5. Hybrid Optical Switching

Hybrid optical switching (HOS) has garnered significant interest in recent years due to its potential to enhance overall network performance and facilitate substantial cost reductions [23]. HOS integrates optical circuit, burst, and packet switching within a single network, assigning each application to the optical transport method that optimally meets its traffic demands, hence facilitating service differentiation at the optical layer. Additionally, HOS anticipates the implementation of two concurrent optical switches. An optical switch with moderate speed and minimal power consumption is employed for transmitting circuits and prolonged bursts, while a rapid optical switch is utilized for packet transmission and brief bursts [24]

1.3. Literature Review

In 2000 Y.-K. Kuo et al. [25] proven numerically that Cr:YSO serves as an efficient solid-state saturable absorber Q-switch for the ruby laser at 694.3 nm, the tunable alexandrite laser from 700 to 818 nm, and the tunable Cr:LiCAF laser from

725 to 840 nm. These passively Q-switched laser systems are robust, resilient, and cost-effective. They can be exceedingly beneficial when compactness is a principal consideration.

In 2001 Y.-K. K. Y.-K. Kuo et al[26]. studied the passive Q-switching performance

of the tunable Cr: LiCAF laser utilizing the Cr: YSO solid-state saturable absorber is examined numerically. The modeling findings indicate that Cr: YSO can serve as an efficient saturable absorber Q-switch for the tunable Cr: LiCAF laser over its whole tuning spectrum from 725 nm to 840 nm.

In 2002, C.-K. Chang et al.[27] The study investigates the optical performance of Cr:YSO Q-switched Cr:LiCAF and Cr:LiSAF solid state lasers, developed by Payne et al. These transition-metal vibronic lasers have broad emission spectra, long lifetimes, low nonlinear refractive indices, low thermal lensing, and low excited state absorption. The results show that the Cr:YSO can effectively serve as a saturable absorber Q switch for the tunable Cr:LiCAF laser over a significant portion of its tuning range.

In 2005, H.-F. Chen et al. [28]the passive Q-switching performance of the tunable Cr: YSO Q-switched Cr: LiCAF laser is numerically studied with the Runge-Kutta method. From the simulation results we conclude that better passive Q-switching performance can generally be obtained with a higher Cr: YSO ground-state absorption and a higher pumping rate. The simulation results show that the Cr: YSO is an effective saturable absorber for the Cr: LiSAF laser over a major portion of its tuning range due to the high Q-switch absorption to laser emission cross-sectional ratio. With a typical laser configuration, a Q-switched laser pulse of 10 mJ in 17 ns at 850 nm is obtained when R = 0.62, Na_0=2.7×10^{16} s^{-1}, and Rp = 4.5×10^{21} s^{-1}.

In 2007, S. N. A.-W. M. Mutter [29]used the passively Q-switching method for chromic solid-state lasers with Cr^{4+}:Y_2SiO_5 solid-state crystal. The saturable absorber crystal properties are studied, including molar extinction coefficient, coupling coefficient, optical density, ground-state absorption cross-section, and Q-switching efficiency. The Cr $^{4+}$: Y_2SiO_5 Q-Switched Cr: LiSAF laser has better passive Q-switching performance than other laser systems. The study indicates that increased pumping rates result in elevated values of parameters like ε, Ka, power, and η. Nonetheless, augmenting output coupler reflectivity diminishes the molar extinction coefficient, coupling coefficient, output laser power, and Q-switching efficiency.

In 2010 H. N. Van et al. [30] numerically investigated the characteristics of diode-end-pumped passively Q-switched solid-state Cr^{3+}: LiSAF lasers. A Cr^{4+}: YSO crystal is used as an intra-cavity saturable absorber. obtained results indicate the influences of resonator and pumping parameters on the characteristics of passively Q-switched solid-state Cr^{3+}: LiSAF laser. Particularly, numerical investigations are done in respect to the Cr^{3+}: LiSAF laser medium of a very wide gain spectrum from 700 nm to 920 nm. Using a CW diode pumping at 670 nm and a Cr^{3+}: LiSAF crystal of 3 mm long. A stable generation of Q-switching nanosecond Cr^{3+}: LiSAF laser pulse at 850 nm is obtainable with a pulse energy of about 2 mili-joule.

In 2014 N. Van Hao et al. [31]The study examines the performance of a passively Cr:YSO Q-switched Cr:LiSAF laser at different power levels. The results show that the loss of the laser is large when intra-cavity light intensity is weak, with an initial value of 1.78×10^{18} ions. The gain is greater than the loss, and the intra-cavity light intensity builds up due to noise, depleting the laser population inversion density. The loss decreases as the intra-cavity light intensity increases.

The laser gain is smaller than the total loss, and the Q-switched laser pulse is exhausted and disappears rapidly. The first Q-switched pulse is developed at 21.35 ms after pumping, with a constant time interval between adjacent pulses. The numerically obtained results show the bandwidth of integrated laser spectrum to be 1.15 nm, a pulse width of 178 ns and a pulse energy of 1.71 mJ.

In 2014 A.-K. M. Salih et al.[32] The numerical solution of rate equations mathem-

atical model was used to investigate the impact of the absorption cross section of a saturable absorber on the behavior of passive Q-switching laser pulse. Studied the passive Q-switching of theCr^{+4}: $BeAl_2O_4$ (alexandrite) laser using the yttrium silicate Cr^{+4}: Y_2SiO_4 (Cr: YSO) solid state saturable absorber. The study reveals that the behavior of pulse energy, starting value of population inversion, and laser photon number is scaling up as the ground state absorption cross section of a saturable absorber increases, while the behavior of pulse length is scaling down.

1.4. Objective of Research

The aim of this research is to improve the performance of a Cr: LiSAF laser operating in passively Q-switched regime using Cr: YSO as a saturable absorber. This is achieved by determining the optimal values of three critical parameters in the rate equations are:

1. The excited state absorption cross-section to the ground state absorption cross-section of the saturable absorber molecules (β).
2. The saturable absorber decay rate (γ_a).
3. Photons losses inside the laser cavity (γ_c).

Optimization techniques are employed to identify these values and to investigate the in fluence of each parameter on the output pulse characteristics.

Chapter Two

Theoretical part

2.1. Introduction

This chapter introduction the fundamental concept behind the Q-switching theory. The difference the two main types of Q-switching (active and passive) has also been studied. Then, the type of the Q-switched active medium laser, Cr: LiSAF is discussed. After that, the saturable absorber materials and their types were reviewed, including the Cr: YSO saturable absorber. Finally, a model of rate equation is presented.

2.2 Q-Switching in Lasers and its Applications

LASER is an abbreviation for "Light Amplification by Stimulated Emission of Radiation" [33]. The laser work to enhancing or amplifying light signals after they are generated by (1) stimulated emission and (2) optical feedback [34]. One method of lasers is quality factor switching (Q-switching). Q-switching is employed to generate substantial laser pulses within a cavity. This is accomplished by obstructing the cavity from lasing by the introduction of losses, preventing the attainment of the laser threshold. The energy is retained as excited electrons until the losses are abruptly eliminated. Subsequently, the substantial gain will generate an oscillating field within the cavity [35]. Since the attributes of these pulses have facilitated advancements in laser applications across numerous domains, including material processing[36], and biomedicine [37], terahertz generation, remote sensing, precise measurement, and spectroscopy[21, 38-40], high-precision processing, laser medical therapy, spatial detection, radar technology, and laser communication [41-43].

Efforts persisted to enhance pulse parameters (energy and duration) about the quality factor of conversion technology, categorized into:

Efforts persisted to enhance pulse parameters (energy and duration) about the quality factor of conversion technology, categorized into:

1- Empirical investigations concerning the advancement of qualitative factor converter technology switches.

2-Theoretical investigations aimed at enhancing the comprehension of factors associated with pulse creation and its specifications will be elucidated in depth through the establishment and development of mathematical models for rate equations.

2.3. Quality Factor (Q)

The Q factor quantifies the extent to which light from the laser's gain medium is fed back into itself by the resonator and it is represented by the Equation[44].

$$Q = 2\pi * \frac{\textbf{Energy stored at resonator in cycle}}{\textbf{Energy depleted at resonator in cycle}} \qquad (2\text{-}1)$$

The quality factor can also be defined by the geometric characteristics of the resonator and the optical properties of the active medium, for instance, a resonator of length (L) cm, with mirror reflectivities R_1 and R_2, and an active medium possessing an absorption coefficient of unit length (α_c) cm, assuming (E_o) represents the energy at time (t=0). Upon completing one cycle within the resonator, the residual energy in the resonator is equivalent to[45].

$$E_{(t)} = E_o R_1 R_2 \exp(-2\alpha_c L) \qquad (2\text{-}2).$$

The duration necessary to finalize one cycle is equivalent to

$$t = \frac{2n_o L}{C}$$

where (n_o) denotes the refractive index of the effective medium, C represents the speed of light.

The quality factor technique allows the conversion of the quality factor (Q) from its minimum value, indicative of maximal energy loss, to its maximum value, representative of minimal energy loss. This must be executed promptly and abruptly; hence, it may be asserted that this technique the primary factor is the degree of control over optical losses within the resonator[46, 47]. This is achieved by inserting a shutter of various forms within the resonator to get a maximum state of inverse population, after which the shutter is rapidly and abruptly opened, resulting in the generation of a giant pulse[35].

There are two conditions for effective Q-switching:

1- The pumping rate must exceed the spontaneous decay rate of the upper lasing level; otherwise, a sufficiently enough population inversion cannot be established.

2-The Q-switching mechanism must function swiftly relative to the buildup of laser oscillation; otherwise, the oscillation would accumulate gradually, resulting in a prolonged pulse with less peak power. Practically, this implies that the switch should preferably function within around a nanosecond or so[48].

Early in the optical pumping process of the active medium, the value of (Q) is low (the amount of photon loss is high). Due to this high loss value and the continuation of pumping, there is a good opportunity for the inverse distribution to become high through continued collection in the upper excited laser plane,). After a period of time, the duration of which is determined by the nature or type of shutter used, the value of (Q) is converted to a high value by making the photon loss as low as possible, while the inverse distribution has become high. This rapid and sudden decrease in photon loss generates laser oscillations, which ultimately produce a short pulse estimated at nanoseconds. It should be noted that the pulse

energy during key operation is less than its energy during normal operation, but its short duration makes its power high, as shown in Figure(2-1) [49].

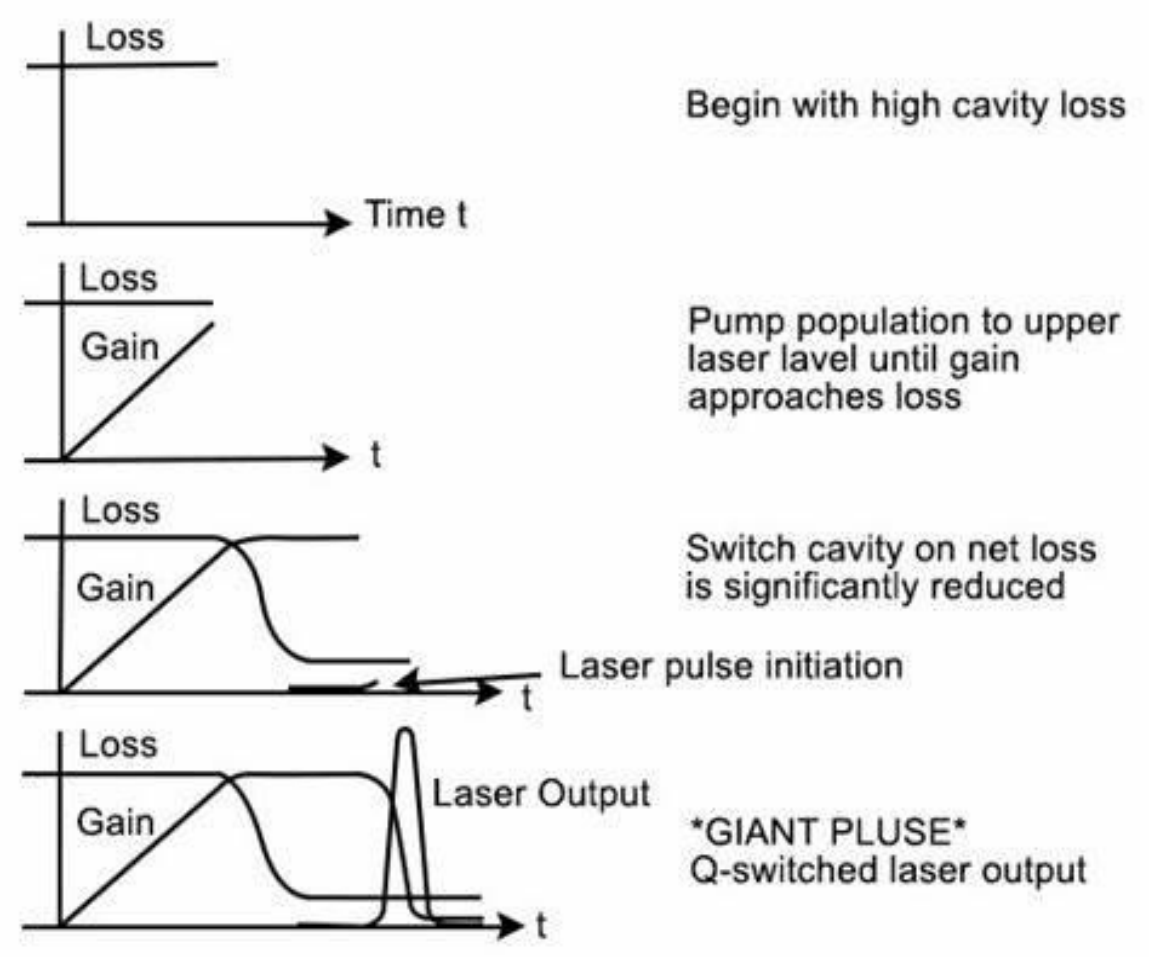

Figure: (2-1) Development of Q-switched pulse[49].

2.4. Methods of Q-Switched Laser

2.4.1. Active Q-Switching

Active Q-switching employs an externally-modulated Q-switch, enabling adaptable repetition rate modifications and temporal synchronization [27]. The electric pulse-driven modulators enable the laser cavity to alternate between high-loss and low-loss states, therefore generating high-quality Q-switched pulses [50].

The energy of the output pulse and its duration are contingent upon cavity loss and the energy accumulated in the gain medium, which is associated with pump power and repetition rate[51]. The benefit of the active Q-switch is its straightforward regulation of the pulse repetition rate and, consequently, the pulse width; nevertheless, its drawback is the necessity for an optical modulator[51]. It is divided into three types:

A. Rotator Mirror Method

In this mechanical configuration, one laser mirror is stationary, akin to a traditional laser, while the second mirror rotates at high velocity, as shown in Figure (2-2). Although the two mirrors are not parallel, the hypothetical switch can be regarded as being in the 'off' position (the cavity exhibits low Q); during the brief interval when the mirrors are parallel, the 'switch' can be perceived as being in the 'on' position, allowing light to oscillate within the cavity (high Q). An electrical trigger synchronizes the flash bulb to ignite at the precise moment corresponding to the revolving mirror [52]. The advantages of this method are simple and affordable devices that can be employed at any wavelength. The undesirable side of this method is that it requires routine maintenance owing to their mechanical degradation and propensity to emit several pulses at a very moderate velocity[53].

Figure: (2-2) Rotator mirror method of Active Q-Switching [52].

B. Acousto-Optic Method

Acousto-Optic (AO) diffraction is extensively employed for beam control, and AO modulators utilizing this phenomenon serve as Q-switches in lasers [54]. The phrase "acoustic-optical" describes the effect of a sound wave on a light wave, exemplified by the phenomena of photoelasticity, which alters the optical characteristics of an optically transparent material under stress. The propagation of sound waves in an optically transparent media induces a periodic alteration in the refractive index , causing the medium to function as a diffraction grating [55]. As seen in Figure (2-3).

Currently, single crystals of germanium (Ge) and paratellurite (TeO_2) serve as the primary AO modulator materials throughout the critical wavelength range of 3 μm. The investigation of efficient materials for use at 3 μm has persisted for over 20 years since their implementation as AO modulators[56], The germanium-based acousto-optic Q-switch is extensively utilized in the 10-μm CO2 laser for optical spectroscopy and environmental monitoring [57]. When the radio frequency driver (RF driver) is operational, the entry of sound waves into the transparent medium utilized as a switch to alter the quality factor induces a change in the medium's refractive index, resulting in the diffraction of incident light[58]. Due to a significant proportion of light deviates from its trajectory with high diffraction orders, resulting in reflection in directions distant from the return path to the laser medium. This occurs due to the light striking the reflecting mirror at angles other than perpendicular, leading to increased photon loss and a reduced value of (Q). Consequently, this presents a favorable opportunity for achieving high population

inversion with continuous optical pumping[55]. The AO Q-switching approaches have a small pulse width and elevated repetition rate. A downside is that the sound wave's influence persists in the substance for a duration after the frequency wave is deactivated[53].

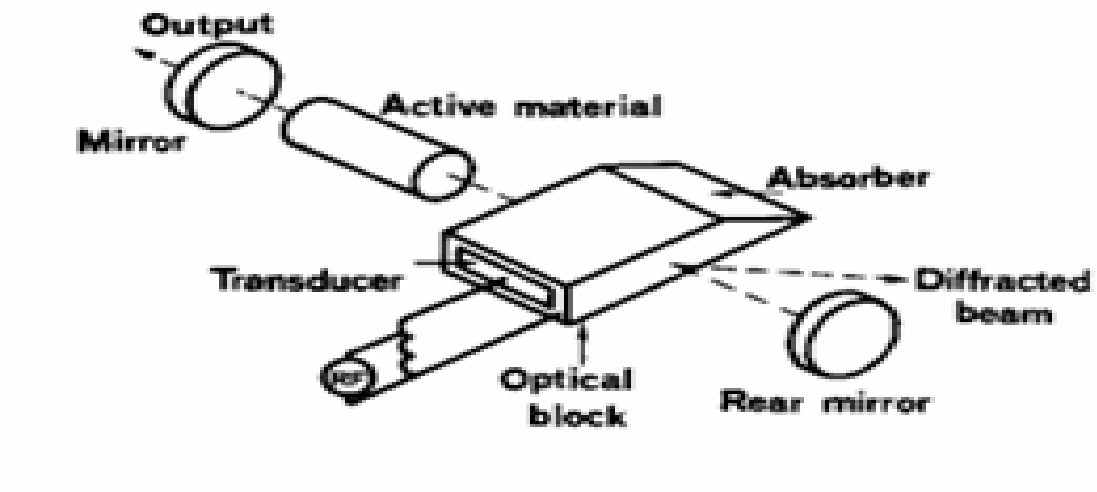

Figure: (2-3) Schematic of an acoustic-optic modulator used for Q-Switching[59].

C. Electro-Optic Method

The increasing diversity of electro-optic materials has led to their widespread application as Pockels cells for Q-switched production of high peak power pulses in solid-state lasers. Initially, water-soluble crystals of potassium dihydrogen phosphate (KDP) and its isomers were extensively utilized in the longitudinal mode, namely when the electric field was oriented parallel to the path of the optical beam[60]. This may be accomplished using lithium niobate (LN, LiNbO3) in a transverse electrode configuration, with light traveling along the optical axis[61]. The electro-optic materials are depicted in Figure (2-4). The light emitted by the laser medium is randomly polarized, but subsequently becomes vertically polarized

by the polarizer. When a DC voltage is given to the electro-optic modulator, it functions as a quarter-wave plate, transforming the vertically polarized light entering its left side into circular polarization. The polarization direction is inverted upon reflection from the mirror. Light entering the right side of the electro-optic modulator is transformed to horizontally polarized light, which cannot pass through the vertical polarizer. This results in significant cavity loss, hence producing a poor Q factor. Upon removal of voltage from the electro-optic modulator, it no longer alters the polarization, resulting in a high cavity Q[55]. This type of switches is expensive[52].

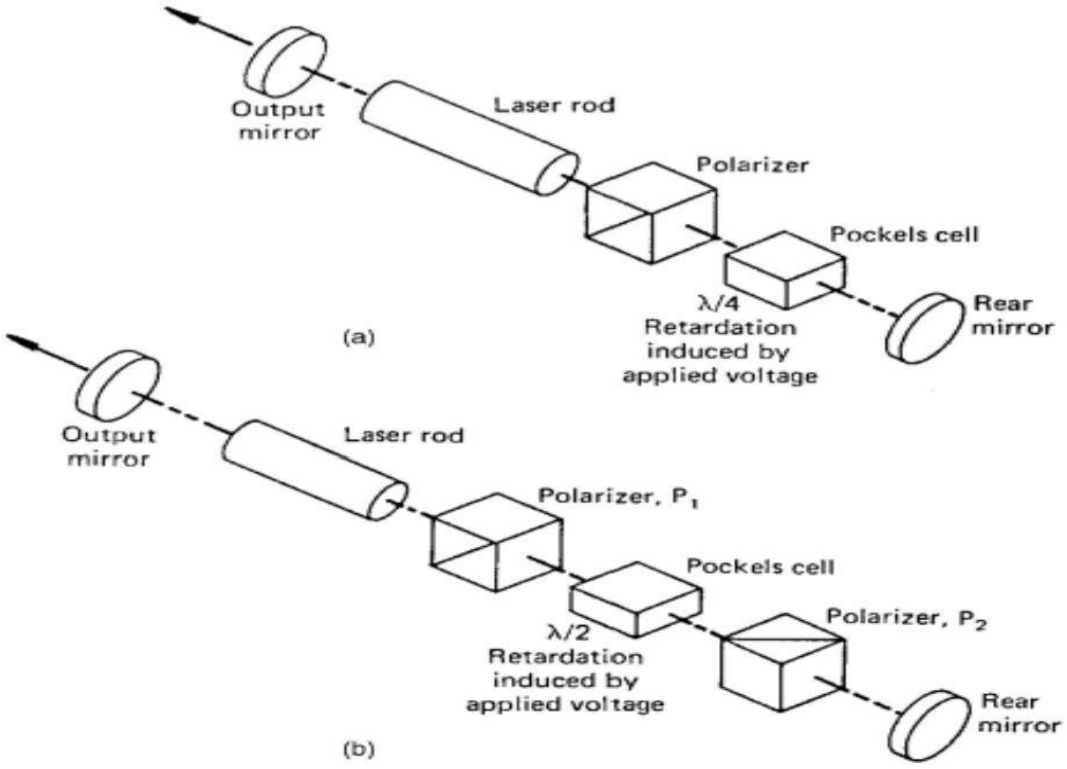

Figure: (2-4) Electro-optic Q-Switching [55].

2.4.2. Passive Q-Switching

The predominant pulsed lasers employ passive Q-switching, wherein a nonlinear optical component known as a Saturable Absorber material (SA) converts the laser's continuous output into a sequence of laser pulses by regulating loss in an oscillator[62].

Generate high-power laser pulses using the passive switching approach; the stages are as follows [63]:

1- Upon pumping the active medium, population inversion is established, and the output laser is hindered by maintaining elevated resonator losses (low Q factor).

2- The passive Q-switch incurs considerable loss, inhibiting the initiation of laser activity in the absence of a feedback system.

3- The power often increases exponentially until the gain reaches saturation. The feedback process is then maintained by swiftly alternating the SA from low to high Q-value [64].

Passive Q-switching has garnered considerable interest for its potential to provide a small and cost-effective alternative, such as semiconductor saturable absorber mirrors [65]. Saturable carbon nanotube pipettes were employed for Q-switching. (SA) is a conventional optical component that modulates loss in an oscillator. A nonlinear effect reliant on laser intensity is employed to achieve a saturable absorber (SA) that responds immediately to intensity changes. According to the SA, a laser pulse incurs less loss with elevated intensity. Consequently, a more intense segment of a laser pulse intensifies significantly, and the temporal length diminishes during the saturable absorption process [62]. Passive Q-switches rely on a process referred to as saturable absorption (SA). This phrase refers to a material's capacity to absorb a specific quantity of light at a designated wavelength before reaching saturation, resulting in temporary transparency. Consequently, if a

saturable absorber material is positioned within the laser cavity, it will absorb all naturally produced photons until saturation is achieved [66]. Passive Q-switched solid-state lasers are optimal for scientific and industrial applications, owing to their design simplicity, reliability, cost-effectiveness, and compactness [67]. This method, utilizing eye-safe lasers, has garnered significant interest due to its use in several fields such as laser surgery and remote sensing. Consequently, much work has been dedicated in recent years to the

development and enhancement of doped stolite glass emitting at wavelengths ranging from 1950 to 2100 nm [68]. Without a dispersion control mechanism, the resultant pulse duration is determined by the equilibrium between pulse shortening from saturation absorption and pulse broadening from dispersion. The pulse duration is mostly dictated by the spectral bandwidth of the laser pulse, measuring[62]. The transform-limited pulse duration represents the minimum pulse length attainable for a specific spectral bandwidth[62]. The passive Q-switched method is an alternative technology for generating a portable and potent laser source that emits short-range, high-intensity Q-switched pulses[69-72].

This technique allows the emission of significantly shorter pulses from the cavity in both directions. This is accomplished by integrating two elements: a gain-providing laser amplifier and a nonlinear loss component[73].

The efficacy of that technique is contingent upon the characteristics of the absorber substance employed:

1. The nonlinear reduction in absorbance corresponding to the rise in incident light intensity[74].

2. The absorption spectra of the absorber materials corresponds to the emission spectrum of the active medium[75].

This technique is distinguished by its straightforward integration within the resonator, cost-effectiveness, and independence from synchronization with the pumping process or electronic control circuits. Consequently, it has undergone further advancement through the incorporation of various liquid and solid switches, molecular gases, and semiconductors, as illustrated in table (2-1).

Table (2-1): Effective medium and saturable absorber material[76-81].

Effective medium	Wave length	Saturated absorbent material
Erbium-doped fiber laser (EDFL)	1564 nm	1- (2-hydroxy-1,4-naphthoquinone), a natural dye material
	1558.92nm, 1557.98 nm and 1558.51nm, respectively	2-graphene, single walled carbon nanotubes (SWCNT) and multi-walled carbon nanotube (MWCNT)
Er–Yb: glass	1.53 μm	(Co^{2+}: $MgAl_2O_4$) solid material
Nd: YVO_4	1341.5 nm	few-layer Platinum diselenide ($PtSe_2$)
Nd: GYAP	1080.4 nm	β-Ga_2O_3 crystals
Cr: ZnSe	2.5 μm	Semiconductor Saturable Absorbing Mirror (SESAM)

Theoretical analysis is necessary to create or regulate the specifications of a high-power laser pulse. The enormous pulse signifies a physical understanding of the interrelations among variables associated with fundamental elements in the pulse production system, hence producing mathematical correlations that elucidate this understanding. Subsequently, use these mathematical relationships to the actual

computations to derive findings that facilitate the assessment of their alignment with practical reality.

The fundamental elements of the examined system (laser system) are defined by the following:

1) Pumping (pumping energy into the active medium).
2) The effective medium.
3) Resonator.
4) Saturable absorber material (the passively switch for quality factor conversion).

2.5. Pumping

Laser pumping is the process of transferring energy into the laser gain medium to achieve the necessary population inversion ΔN21. The energy is absorbed by the medium, resulting in the excitation of its atomic states. Pump energy is often supplied as light or electric current, however more unconventional sources, like chemical or nuclear processes, have also been utilized [82].

1) Optical Pumping

Optical pumping of lasers often pertains to the excitation of liquid (dye) lasers and dielectric solid-state lasers, facilitated by either flashlamps or alternative lasers. The predominant flashlamp forms utilized for laser pumping are narrow, cylindrical quartz tubes equipped with metal electrodes at both ends, filled with a gaseous medium like xenon that acts as the radiating substance within the lamp. A voltage is supplied across the flashlamp electrodes, causing current to flow through the gas, which populates the excited energy levels of the atoms, resulting in strong light emission [82].

2) Electrically Pumping

Typically, it is executed by a continuous wave, radio-frequency, or pulsed current traversing a conductive medium, such as an ionized gas or semiconductor, typically achieved with a sufficiently powerful electrical discharge [59].

3) Chemical Pumping

Chemical reactions serve as a power source in chemical lasers. The energy produced by these reactions is utilized to energize the active medium and attain population inversion. This enables exceptionally high output powers that are challenging to achieve using alternative methods[59].

4) Others Pumping Ways

Nuclear fission is utilized in unusual nuclear pumped lasers (NPL), directly harnessing the energy of fast neutrons emitted from a nuclear reactor[83]. The aforementioned pumping processes optical, electrical, and chemical pumping are not the exclusive methods available for laser pumping. A process akin to optical pumping occurs when the medium is stimulated by a beam from an X-ray source (X-ray pumping). Similarly, a pumping process akin to electrical pumping occurs when the medium is stimulated by a beam of electrons from an electron-beam machine (e-beam pumping). Despite the capability of both X-ray and e-beam pumping to provide substantial pump powers or energies throughout a significant volume of active medium, both pumping methods are not commonly employed in practice due to the intricacy of the X-ray or e-beam equipment. It is noteworthy that the shortest wavelength attained in a laser, around $\lambda \cong 1.4$nm, which is at the threshold between the soft and hard X-ray regions, has been realized using the strong X-rays generated by a tiny nuclear explosion. The specifications of this laser

remain classified; nonetheless, it is evident that this pumping setup is not easily replicated in a standard laboratory setting[59].

2.6. Cr: LiSAF Laser

Nowadays, solid-state lasers play a significant role in the laser industry, owing to its numerous advantageous characteristics, including robustness, dependability, safety, user-friendliness, compactness, and cost-effectiveness [84]. Crystal growth of Cr: LiSAF(Chromium-doped Lithium Strontium Aluminum Fluoride) at Lightning Optical Corporation (LOC) commenced in 1991 following the acquisition of a license to cultivate and market this material [85]. Cr: LiSAF gain medium has an extensive gain bandwidth of about 800 nm, enabling complete tunability from 780 nm to 1110 nm and permitting the creation of pulses at the 10-fs level[86, 87]. Furthermore, Cr: LiSAF crystals exhibit minimal passive losses, and the product of their fluorescence lifetime and emission cross-sections is notably high (320 μs x 10^{-20} cm^2)[86, 87]. Consequently, the lasing threshold of Cr: LiSAF lasers can be quite low (a few milliwatts). Moreover, Cr: LiSAF has an inherent slope efficiency of 54%[88], facilitating the development of extremely efficient systems. Finally, it is crucial to note that Cr: LiSAF exhibits extensive and robust absorption bands at 650 nm, facilitating direct excitation by economical red laser diodes [89]. This laser is used in several applications, including generating very short light pulses, acoustic pulse amplification systems, medicine, and spectroscopy[90, 91]

2.7. Resonator

The cavity is specifically designed to provide the requisite feedback for laser oscillation, forming optical structures. The resonator facilitates the amplification

process, generating highly coherent and monochromatic light, thereby enabling the construction of a high-intensity source[92].

The propensity of the laser to oscillate in several patterns arises from the resonator's dimensions being greater than the laser's wavelength[93].

The resonators employed in the laser oscillator typically consist of an open configuration with a pair of mirrors oriented towards one another and perpendicular to the optical axis of the active medium[94].

2.8. Resonator Losses

Photon losses inside an optical resonator refer to the mechanisms by which photons are lost or dissipated from the resonator, reducing its efficiency and performance. These losses can be originated from various factors, including absorption within the cavity materials, scattering due to imperfections or surface roughness, diffraction losses at the cavity boundaries, and imperfect mirror reflectivity. Minimizing these losses is crucial for achieving high-quality (high-Q) resonators [95].

There are many photon losses inside the resonator, including:

2.8.1. Non - Radiative Transmission Losses

Losses resulting from non-radiative transitions occur between layers above the quasi-steady level or beneath the lower laser level (not associated with the laser activity, i.e., the laser transition) [96]. As it happens of spontaneous emission from excited states to lower states, the loss due to spontaneous emission is dispersed throughout all modes of the gap[97].

2.8.2. Diffraction Losses

The electromagnetic field within the resonant gap may experience decay with this loss being ascribed to diffraction occurring at the final ports of the mirrors when the wave oscillates between them. This loss results in an additional loss referred to as diffraction loss for the resonator mode is defined as the energy loss incurred during a single pass[98].

Diffraction losses are quantified by a parameter known as the diffraction loss coefficient, as delineated in equation (2-3) [99].

$$L=-\ln\left(\frac{1}{M^2}\right) \qquad (2\text{-}3)$$

Where:

L: The round-trip loss coefficient is defined as the ratio of the area of the starting wavefront to the area of the wavefront after one complete round trip.

M : It is the magnification factor of the round trip.

The likelihood of diffraction escalates as the wavelength of the electromagnetic beam exceeds the dimensions of the edges that obstruct it [100].

2.8.3. Losses of Non-Uniformity of Reflectivity of the Resonator Mirrors

Due to one resonator mirror being partially reflective and the other fully reflective, the former transmits a fraction of the electromagnetic rays within the resonator during each traversal through the gap. Consequently, the transmittance of this mirror constitutes a significant source of loss in the resonator, thereby preventing laser action unless this loss is mitigated attains the benchmark or exceeds it. Oscillation will not take place unless the gain of the active medium above the loss in the laser (output loss). The gain per traversal of the active medium, defined as the ratio of the outgoing photon flow to the incoming photon flux, is

$$l(\exp[\sigma_T(N_2 - N_1)])$$

then (l) the length of the active medium. Assuming that the sole loss in the resonator is attributable to permeability, then the requisite condition for laser oscillation is [101]

$R_1R_2 \exp[2\sigma_T(N_2\text{-}N_1)L] = 1$ (2-4)

Since R_1R_2: the reflectivity of mirrors (1) and (2) respectively

σ_T :is the cross-section of the permeability(cm).

L : Resonator length.

N_1N_2: the population of levels (1) and (2) respectively.

Thus, the output loss (L_o) is defined by the following equation.

$L_o = \frac{1-R_O}{M^2}$ (2-5)

Where R_o: the peak reflectivity.

M: the magnification factor [102].

2.8.4. Reflection and Refraction Losses

The electromagnetic beam experiences several reflections from the interior walls of the pumping cavities, resulting in significant energy loss prior to the laser output process [103]. When a planar electromagnetic wave impinges upon a boundary between two mediums with distinct refractive indices at a specific angle of incidence, the coefficients of reflection and transmission are contingent upon the components of the incoming polarized light [28].

2.8.5. Absorption Losses

The pumping cavities, composed of core materials with varying refractive indices, may absorb electromagnetic radiation inside prior to their emergence from the partly permeable mirror [103].

2. 9. Saturable Absorber Materials

In a passively Q-switched technique, the selection of a saturable absorber material is a critical design consideration. The material must possess superior qualities within production tolerances, be readily available in the market, and have the appropriate characteristics to facilitate effective Q-switching. The following qualities are summarized below [104]:

1. Significant ground-state absorption cross section to facilitate rapid activation of the Q-switch.

2. The absorption cross section in an excited state should be minimized to reduce residual absorption losses once the Q-switch is saturated (open). To prevent the Q-switch from shutting prematurely, its excited state lifetime must significantly exceed the duration of the output pulse. Numerous varieties of saturable absorber materials may be identified, including the following:

2.9.1. Dye Saturable Absorber

In this context, researchers focused on more efficient developing nonlinear optical materials, particularly organic compounds, which exhibit a remarkable nonlinear optical response conducive to the creation of appropriate ultrashort pulses[105]. Organic materials provide diverse properties that demonstrate significant potential for all-fiber pulsed lasers. Most organic materials have extensive spectrum tunability, little processing costs, and rapid nonlinear responses. The organic group is very environmentally benign and is extensively utilized in the fabrication of novel photonic devices, including thin film transistors, organic solar cells (OSCs), and light-emitting diodes (LEDs)[106]. Moreover, organic groups exhibit straightforward processing that facilitates flexibility in controlling physical attributes. Nevertheless, they have not been substantially researched for fiber laser applications despite their significant promise in this area. An illustration of this is lawsone (2-hydroxy-1,4-naphthoquinone), a natural dye

material suggested and proved as a saturable absorber (SA) for passive Q-switching in an Erbium-doped fiber laser (EDFL) cavity [76].

2. 9.2. Solid Saturable Absorber

All-solid-state pulsed lasers are crucial in scientific research, industry, medicine, information technology, and military applications due to their small pulse width, high peak power, and substantial pulse energy [87, 107-111]. In recent years, the need for ultrashort pulses with elevated average power has surged across several fields, including precision micro-nano processing, biomedicine, scientific research, and ultrahigh-speed optical communication [112-117]. As semiconductor laser technology matures, laser diode pumped solid-state lasers (LDPSSLs) are emerging as superior laser sources characterized by small design, high efficiency, longevity, and exceptional beam quality [118, 119]. In commercial and industrial systems, the predominant semiconductor saturable absorber mirror (SESAM) is utilized[120, 121]. Which has seen swift development and commercialization in recent decades, finding applications in fiber lasers, solid-state lasers, and thin-slice lasers[122-124]. In recent years, the advent of low-dimensional (LD) materials, encompassing two-dimensional (2D), one-dimensional (1D), and zero-dimensional (0D) materials, presents a novel possibility for the advancement of pulsed lasers.[125-127]. The 2D material denotes atomic layer material, which may consist of a single layer or many layers in thickness. It possesses robust covalent bonds inside the layer and weak interlaminar van der Waals forces. In the absence of interlayer interactions, electron mobility is constrained in two-dimensional systems, leading to the emergence of several novel electrical and optical features in 2D materials. [128, 129]. Graphene is the inaugural monatomic layer material identified, with remarkable mechanical, thermal, electrical, and optical characteristics [130, 131]. Subsequently, topological insulators (TIs), transition

metal dichalcogenides (TMDs), black phosphorus (BP), and perovskite materials were documented[131-133]. Furthermore, the advent of one-dimensional materials like carbon nanotubes (CNTs) and zero-dimensional materials such as quantum dots (QDs) has significantly contributed to the advancement of pulsed solid-state lasers [134, 135] see in Figure (2-5).

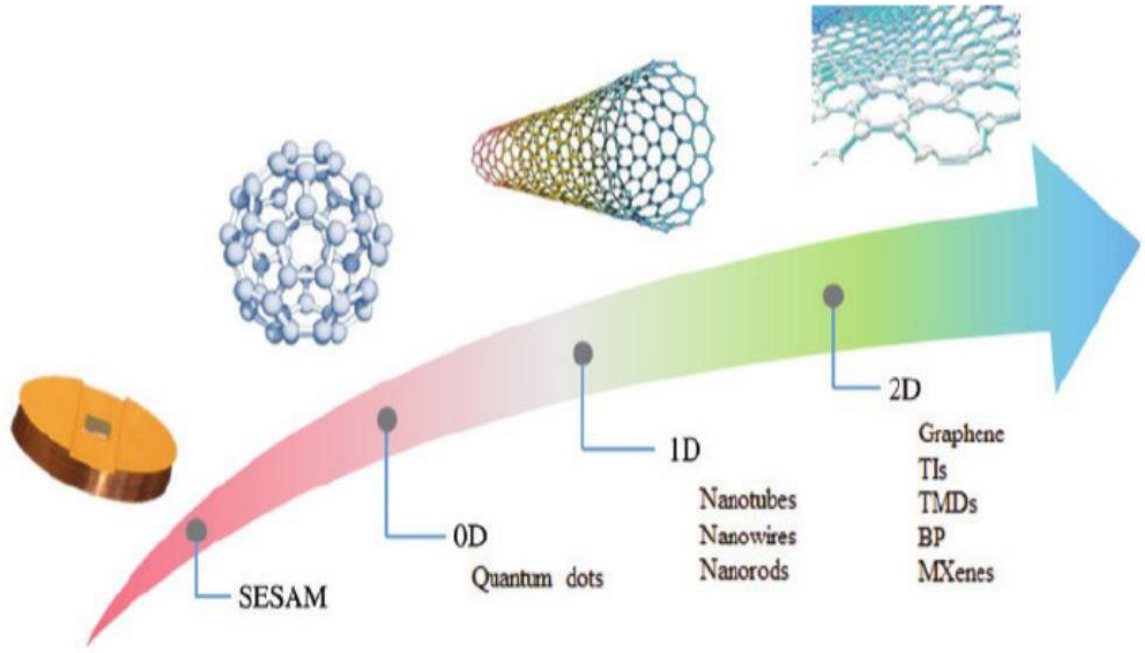

Figure: (2-5) The development of SA ranged from SESAM to LD materials [136].

2.10. Cr: YSO Saturable Absorber

The Cr: YSO (Cr^{4+}: Y_2SiO_5) (Chromium-Doped Yttrium Orthosilicate) is a purely tetravalent chromium system. It is blue in hue and is a biaxial solid-state crystal [137]. Deka et al. published the initial spectroscopic investigations of Cr^{4+}: YSO and the detection of laser action from 77 to 257 ºK in 1992. Kück et al. also documented room-temperature laser operation of Cr^{4+}:YSO [27]. It was experimentally established that, the Cr:YSO crystal may also function as a saturable absorber Q-switch for the tunable Cr:LiSAF laser[30]. The material possesses a melting point of 2070 ºC, a chromium atom concentration of 9.7 x 10^{19}

atoms/cm³, a density of 4.6 g/cm³, a refractive index of 1.8, and a damage threshold of 30 J/cm² [25, 138]. It possesses four absorbance bands with peaks at around 390 nm, 595 nm, 695 nm, and 750 nm [25] as shown in Figure (2-6). Its absorption spectrum encompasses the visible and near-infrared spectral regions, hence enabling its application as a saturable absorber. Q-Switch for ruby, alexandrite, Cr:LiCAF (Chromium-Doped Lithium Calcium Aluminum Fluoride), and Cr:LiSAF lasers[25].

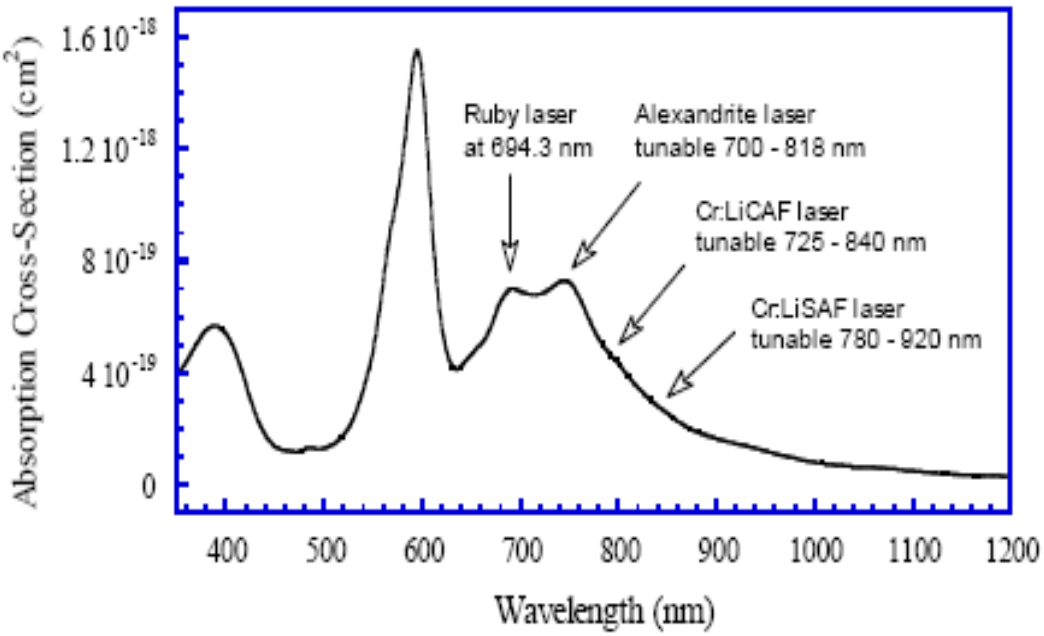

Figure: (2-6) $Cr^{4+}:Y_2SiO_5$ absorption spectrum[25].

The absorption process within it may be delineated as follows Figure (2-7). Most of the molecules located in the ground state level, ions absorbed the stimulated photons and excited to level (3), the ions relax fast to temporal equilibrium level (2) of excited state (τ_{32} very short), ions in level (2) absorbed the incident photons and excited to level (4) and relax to level (2), within stay the ions in the first excited state (relaxation time τ_1 relatively long) they may be excited to level (4) (relaxation time τ_3 very short) ions back to level (2).That make all the molecules in the first excited state advert in the absorption activity to this level, the absorption will increase with increasing the incident photons in the

saturable absorber. So the absorption will not stop unless transfer the majority of ions to the excited state[139].

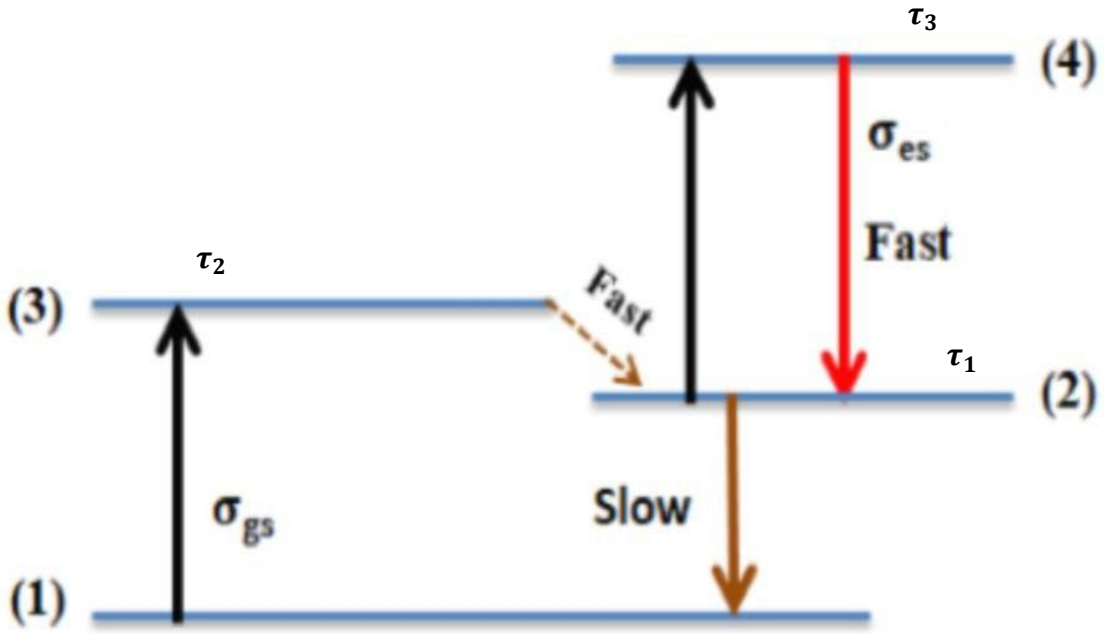

Figure: (2-7) Energy level diagram of Cr+4: YSO[140].

This material is suitable for use in high-axial-resolution optical coherence tomography (OCT)[141-143], remote sensing, precision cutting, marking materials, and in medicine to treat skin diseases[28, 31, 144].

2.11. Rate Equations for Passive Q-Switching

This thesis focuses on passive Q-switching technique, which employs some solid materials. Used a system of rate equations for four energy levels.

This model will appropriately depict the rate equations for a passive Q-switched laser based on the absorption process of the saturable absorber in this system. This model considers the contribution of the first excited state absorption of the stimulated photons as shown in the Figure (2-7). Consequently, this results in a reduction in the cavity photon number. The current formulation of the rate equation

for passive Q-switching utilizing a saturable absorber as a four-level system may be expressed as[145].

$$\frac{dn}{dt}=[K_g N_g \ - \ K_a N_a - \beta K_a N_{au\_} \gamma_c]\text{n} \qquad (2\text{-}6)$$

Equation (2-6) delineates the rate equation for the cavity photon number (n). The first term denotes the temporal increase rate of the signal attributable to stimulated emission, which serves as the source of laser photons. The second component of this equation denotes the rate at which the ground state of the saturable absorber absorbs laser photons. The third term denotes the rate at which laser photons are absorbed by the first excited state of the saturable absorber. The last element of this equation denotes the reduction in signal energy resulting from the interplay of internal cavity losses and cavity output coupling.

$$\frac{dN_g}{dt}= R_p \ - \ \gamma_g N_g \text{ - } 2 * K_g N_g \text{n} \qquad (2\text{-}7)$$

Equation (2-7) delineates the rate equation for the gain medium exhibiting population inversion (N_g). The first component denotes the pumping rate, which contributes to the augmentation of population inversion in the gain medium, whereas the second term signifies the rate of decline of population inversion resulting from spontaneous emission. The last limit represents the rate of decrease in the population inversion of the active medium due to stimulated emission.

$$\frac{dN_a}{dt} = \gamma_a \ N_{au} \ - K_a N_a \text{n} \qquad (2\text{-}8)$$

Equation (2-8) delineates the rate equation for a saturable absorber molecule in its ground state (Na). The first component denotes the rate of rise in decay from the first excited state, whereas the second term indicates the rate of reduction in the number of saturable molecules in the ground state owing to incoming photons on the saturable absorber.

$$\frac{dN_{au}}{dt} = K_a N_a\, n - \gamma_a N_{au} \qquad (2\text{-}9)$$

Equation (2-9) delineates the rate equation for saturable absorber molecules in the first excited state (Nau), wherein the initial term signifies the rate of increase in the quantity of saturable absorber molecules at this state, attributable to incident photons that excite molecules from the ground state to the first excited state. The second term represents the rate of decrease in the number of the saturable molecules at the first excited state due to spontaneous decay from the first excited state to the ground state.

Where n is the photon count within the laser resonator.

N_g represents the population inversion(cm^{-3}).

N_a represents the ground state population of the saturable absorber(cm^{-3}).

N_{ao} represents the initial value of Na.

$\gamma_g = 1/\tau g$ represents the effective decay rate of the upper laser state (sec^{-1})

τ_g represents the laser emission lifetime (sec).

R_p represents the pumping rate (sec^{-1}).

K_g is the coupling coefficient between the stimulated photons and the active medium component.

$Ka = 2\sigma ag/\tau_r Aa$ is a coupling coefficient between photons and the saturable absorber molecules.

$\gamma_c = 1/\tau_c$ represents the cavity decay rate, where

$\tau_c = \tau_r/\gamma$ represents the cavity lifetime.

Chapter Three

Optimization

3.1. Introduction

This chapter introduces the concept of optimization in general first. Then, a classification of programming is presented based on linear and nonlinear objective function programming to find the optimal solutions in algorithms. After that, the physical analysis of the rate equations, decision variables, objective functions, and constraints for this study is explained. Finally, the decision of selecting the appropriate technique (Constraint Rosenbrock) for this study is discussed.

3.2. General Optimization

The notion of optimization is now well established in the examination of several difficult decision-making or allocation issues. It provides a notable level of philosophical sophistication that is difficult to contest, and it frequently delivers an essential degree of operational simplicity. Employing this optimization methodology, one addresses a complicated choice issue that entails selecting values for several associated variables by concentrating on a singular objective intended to quantify performance and assess the quality of the solution. This singular goal is optimized (either maximized or reduced, contingent upon the formulation) under the restrictions that may restrict the selection of decision variable values. Isolating and characterizing a specific aspect of a problem, whether it pertains to profit or loss in a business context, speed or distance in a physical scenario, expected return in risky investments, or social welfare in government planning, allows for the application of optimization as an effective analytical framework [146].

Optimization challenges have the following essential components:

- Variables that can assume a wide range of values. The most prevalent forms of variables are real numbers, integers, or binary values (specifically, 0 and 1), but matrix variables are also feasible.

- Constraints that delineate permissible values or ranges for the variables.
- An objective function that quantifies the attractiveness of a certain combination of variables.

The optimization issue involves selecting among all variables that meet the restrictions the values that minimize the objective function [147].

Optimization algorithms may be classified into two primary categories: deterministic algorithms and stochastic algorithms. Deterministic algorithms employing gradients, such as hill-climbing, exhibit a systematic progression and will produce identical solution sets if the iterations begin from the same initial position. Conversely, stochastic algorithms that do not utilize gradients frequently provide varying solutions despite identical beginning values. Nonetheless, broadly speaking, the ultimate values, while marginally distinct, will converge to identical optimal solutions within a specified precision [148]. Optimization techniques can be categorized based on the structure of the issue into:

3.3. Linear Programming

Linear programming focuses on optimizing (minimizing or maximizing) a linear function while adhering to a series of linear equality and/or inequality constraints. The linear programming issue was initially formulated by George B. Dantzig about 1947 [149].

Linear programming is perhaps the most intuitive method for articulating a wide range of problems with minimal effort. A linear programming problem is defined by linear functions of the variables; the objective function is linear in the variables, and the constraints consist of linear equalities or inequalities involving the variables. Those acquainted with various disciplines of linear mathematics may first presume that linear programming formulations are easy due to the more

favorable mathematics and the simpler computations associated with linear issues compared to nonlinear ones. However, they are not the principal causes. Mathematically and computationally, there exist bigger categories of optimization problems beyond linear programming that possess sophisticated theories and for which efficient methods are accessible. The appeal of linear programming appears to reside mostly in the formulation phase of analysis rather than the solution phase and for valid reasons. A significant proportion of restrictions and objectives encountered in practice are unequivocally linear. For instance, if one defines a problem with a budget constraint limiting the total funds to be distributed between two distinct commodities, the budget constraint is expressed as $x_1 + x_2 < B$, where xj (for i = 1, 2) represents the allocation for activity i, and B is the budget[150].

Numerous optimization approaches address the linear optimization issue, namely:

- Simplex
- Graphical
- Interior point
- Revised simplex
- Cutting plane
- Branch and bound
- Dual simplex

3.4. Nonlinear Programming

The primary challenge in nonlinear programming is to minimize or maximize a specified function of several variables while adhering to a finite number of inequality and/or equality constraints. Numerous theoretical and practical issues that may be formulated as nonlinear programming problems emerge across several domains, including economics, game theory, operations research, statistics, and

physics. Nonlinear programming is a domain of optimization theory that addresses static, finite-dimensional optimization problems, focusing on computational elements. The term "mathematical programming" is also utilized. The expression was initially established by Robert Dorfman in 1949. as per the recollections of G.B. Dantzig about the inception of Linear Programming [151].

These strategies are categorized into four types based on the structure of the problem they aim to address:

1- Single Variable Unconstrained

Unconstrained optimization issues arise in several domains, especially when the problem formulation is straightforward. More intricate formulations frequently incorporate explicit functional limitations. Many limited issues are often transformed into unconstrained problems, such as by the application of barrier functions, for instance, the analytic center problem in (dual) linear programming [152]. The Regula Falsi method, the Bolzano method, and the Newton method are classical techniques for determining the roots of equations in a single variable [153].

2-Single Variable Constrained

Constrained optimization comprises strategies aimed at systematically and effectively identifying the optimal solution to a problem defined by several alternative solutions under specified restrictions. It involves optimizing an objective function that quantifies a measure of significance to the decision maker, constrained by limitations that restrict their options. The optimization of the objective function is achieved by methodically choosing input values for the decision from a permissible set and calculating the objective function iteratively, until the choice produces the optimal value for the objective function [154]. This

search pertains exclusively to a solitary independent variable constrained by specific limitations. The process for this category starts with the initial limits on the independent variable. The Fibonacci method is the most used single-variable search approach[155].

3-Multivariable Unconstrained

Techniques for peak-finding issues encompass the Steepest Descent technique, the Gradient method, and further approaches that employ Conjugate Gradients. The Conjugate Gradient techniques were initially presented by Davidson and then refined by Fletcher, Powell, Reeves, A1-Baali, Touati and Storey. The Conjugate Gradient techniques claim that near a minimum; a function may be accurately represented by a positive definite quadratic form. This methodology is employed for resolving unconstrained nonlinear multivariable problems, including the Hooke and Jeeves Pattern Search and the Nelder and Mead method. The Hooke and Jeeves method involves exploring the local characteristics of the objective function inside the space and thereafter progressing in a beneficial path to minimize the functional value. This technique is one of the most straightforward and effective approaches for addressing unconstrained nonlinear minimization issues[156, 157].

4-Multivariable Constrained

Numerous scientific and engineering challenges include nonlinear systems that are subjected to numerous restrictions, including input and output constraints. Many control systems are subject to input restrictions such as input saturation, hysteresis, or dead-zone; violations of these constraints may lead to undesirable performance outcomes. The input saturation restriction is a critical input limitation often encountered in several industrial control systems. Consequently, several investigations have been conducted on the analysis and control design of systems with saturation limitations. Many control systems impose limits on their outputs or

states due to physical limitations, performance criteria, and safety standards. The Barrier Lyapunov function (BLF) is a useful way for addressing such difficulties, since it produces a value that tends toward infinity as its arguments reach certain boundaries [158].

The following methods are representing central methods for this category:

- Genetic Algorithm (GA).
- Ant Colony Algorithm (ACA).
- Particle Swarm Algorithm (PSO).
- Box Algorithm.
- Constrained Rosenbrock Algorithm.
- Ronen Algorithm.
- Fiacco and McCormick Algorithm.
- Differential Evolution Algorithm.
- Simulated Annealing Algorithm.
- Harmony Search Algorithm.
- Firefly Algorithm.

3.5. Optimal Solutions in Algorithms

An optimum solution in algorithms denotes a resolution that attains the most favorable result for a certain problem based on established criteria. The notion of an optimal solution revolves around identifying the outcome that yields the greatest benefit, minimal cost, or utmost efficiency, typically accomplished through mathematical techniques or specialized algorithms, including linear programming, search algorithms, or other optimization methods. In the realm of algorithms, an

optimum solution entails the equilibrium of available resources with defined objectives, resulting in the most efficient outcome.

Table (3-1): Optimization technique classification [159].

Technique	Single Variable	Multivariable	Unconstrained	Equality Constrained	Inequality Constrained	Linear Objective Function	Derivative Required	Integer Solutions	0-1 Integer Solutions	Maximum extreme	Minimum extreme	General Solutions
Simplex		*		*	*	*				*		*
Revised Simplex		*		*	*	*					*	*
Integer Programming		*		*	*	*		*			*	
Zero-One Programming		*		*	*	*			*	*	*	
Coggin	*		*							*		*
Fibonacci	*				*						*	*
Nelder-Mead		*	*								*	*
Hook-Jeeves		*	*								*	*
Rosenbrock		*	*								*	*
Powell		*	*								*	*
Fletcher-Reeves		*	*				*				*	*
Fletcher-Powell		*	*				*				*	*
Box		*			*					*		*
Constrained Rosenbrock		*			*					*	*	*
Rosen		*			*		*			*		*

Fiacco-McCormick		*		*	*		*				*	*
Constrained Fletcher-Powell		*		*	*		*				*	*

3.6. Physical Analysis of Rate Equations

The equations (2-6 to 2-9) require numerical solutions to obtain the behavior of a specific Q-switched laser system. Consequently, critical aspects like the initial, threshold, and final laser population inversion, the peak photon count within the laser resonator, as well as the output energy and pulse width of Q-switched laser output have been examined through the analysis of these four linked rate equations.

At the initial moment, the majority of saturable absorber molecules exist in the ground state (Nag), indicating that the absorption activity of the saturable absorber is very high at this time $N_a \approx N_{ao}$

$N_{au} \approx 0.0$ and $\frac{dn}{dt} = 0$

Na_o represents the total quantity of saturable absorber molecules, based on these estimates. We get an accurate estimate for the initial value of population inversion in the laser medium (N_{go}) Then from equation (2-6)

$$N_{go} = \frac{K_a N_{ao} + \gamma_c}{K_g} . \qquad (3\text{-}1)$$

After a brief duration, contingent upon the lifetime of the saturable excited state, the

majority of saturable absorber molecules are in the excited state (N_{au}); hence, we can consider

$N_{au} \cong N_{ao,}$ $N_{a\cong 0.0}$ and $\frac{dn}{dt} \approx 0.0.$

By employing this approximation in equation (2-6), we may forecast the threshold population inversion (N_{th}) as following:

$$N_{th} = \frac{\beta K_a N_{au} + \gamma_c}{K_g} . \qquad (3\text{-}2)$$

Typically, the build-up time of a Q-switched laser pulse is significantly shorter than the pumping rate (Rp) and the relaxation time of the active medium (τ_g), allowing for the neglect of the pumping rate and spontaneous decay of laser population inversion during pulse generation. Consequently, from equations (2-6) and (2-7), we derive

$$\int_{n_I}^{n_p} dn = -\frac{1}{\gamma_p}\left[\left(\int_{N_{go}}^{N_{th}} dN_g - \left(\frac{K_a N_a + \beta K_a N_{a_u} + \gamma_c}{K_g}\right)\int_{N_{go}}^{N_{th}} \frac{dN_g}{N_g}\right]\right. \qquad (3\text{-}3)$$

According to equation (3-3), the photon number attains a peak value (n_p) when the population inversion (N_g) equals the threshold population (N_{th}), while N_a approaches zero; hence, we obtain

$$\int_{n_I}^{n_p} dn = -\frac{1}{\gamma_p}\left[\int_{N_{go}}^{N_{th}} (dN_g) - N_{th}\int_{N_{go}}^{N_{th}} \frac{dN_g}{N_g}\right]$$

$$n_p - n_I = -\frac{1}{\gamma_p}\left[(N_{th} - N_{go}) - N_{th}\ln\left(\frac{N_{th}}{N_{go}}\right)\right]$$

But $n_p \gg n_I$, then

$$n_p = -\frac{1}{\gamma_p}\left[N_{th} - N_{go} - N_{th}\ln\left(\frac{N_{th}}{N_{go}}\right)\right]. \qquad (3\text{-}4)$$

Following the emission of the Q-switched laser pulse, the population inversion diminishes to the final value (N_f), which may be employed to compute the output energy of the Q-switched pulse using the subsequent equation:

$$E_{out} = \left(\frac{N_{go}-N_f}{\gamma_p}\right)\left(\frac{N_{go}-N_f}{N_{go}}\right) \times h\nu \quad (3\text{-}5)$$

hν represents the energy of laser radiation. The peak power of the Q-switched laser output may be approximately determined using equation (3-5) as follows:

$$P_p = \frac{n_p h\nu}{\tau_c}\left(\frac{N_{go}-N_f}{N_{go}}\right) \quad (3\text{-}6)$$

$$P_p = \frac{h\nu}{\gamma_p \tau_c}\left(N_{th} - N_{go} - N_{th}\ln\left(\frac{N_{go}-N_{th}}{N_{go}}\right)\right).$$

The pulse duration of the Q-switched laser pulse may be estimated using the following formula [32]:-

$$\tau_{pulse} = \frac{E_{out}}{P_p} \quad (3\text{-}7).$$

3.7. Decision Variables for the Process Under Study

The decision variables of the process, as defined in the problem formulation, are β (the ratio of the excited-state absorption cross section to the ground-state absorption cross section of the saturable absorber), γ_a (the spontaneous relaxation rate of the saturable absorber), and γ_c (the cavity decay rate).

3.8. Objective Function

The determination of optimal passive Q-switching must fulfill four objective functions, which include

1) Cavity photon number (N).
2) Gain medium exhibiting population inversion (N_g). Saturable absorber
3) molecules in the ground state (N_a).
4) Saturable absorber molecules in the first excited state (N_{au}).

3.9. The Constraints

The optimization constraints in this work may be categorized into[32, 138, 160]:

1) The ground state population of the saturable absorber (N_a) must exceed the population of the first excited state (N_{au}) during the rising time. $N_{au} < N_a$.
2) The ratio of the excited-state absorption cross section to the ground-state absorption cross section of the saturable absorber is valued between 0.2 and 0.9.
3) The relaxation rate of the saturable absorber is valued between 1×10^6 and 7×10^6
4) The cavity decay rate is valued between 1×10^8 and 7×10^8.

3.10. The Specifications for the Suitable Technique of This Study

The problem formulation encompasses decision variables, objective functions, and the physical analysis of rate equations. The issue possesses the subsequent characteristics.

(1) Nonlinear.

(2) Multivariable.

(3) Constrained.

The technique must also accomplish the following conditions:

I. Find the maximum and minimum solution. II. Gives general solution.

Among the optimization strategies, it has been found believe that the Constrained Rosenbrock Method is the best appropriate methodology to address this problem, since it fulfills the necessary requirements and contexts.

3.11. Constrained Rosenbrock Technique

The Rosenbrock Technique determines the maximum or minimum value of a multivariable function inside a defined domain[161]. The Rosenbrock function, also referred to as the "Banana function" because to the unique form of its contour lines, see Figure (3-1), the x, y axes represent the variables (x, y), while the z axis represents the value of the Rosenbrock function f(x, y). The Rosenbrock function is defined as:

$f(x, y) = (a-x)^2 + b(y-x2)^2$

where a=1and b=100 are standard parameter values [162].

A restricted optimum denotes a solution in which certain variables are situated near the boundaries of their permissible ranges. The constraints under examination are equality constraints, which are assumed to relate to both the functions of the independent variables and the independent variables themselves; hence, the goal is to maximize (or minimize) a function. $f(x_u \ldots x_n)$ of n independent variables $x_u \ldots x_n$ subject to m constraints of the form $g_k < x_k < h_k$, k=l,...m and the lower and upper constraints g_k and h_k are either constants or functions of $x_u \ldots x_n$[161].

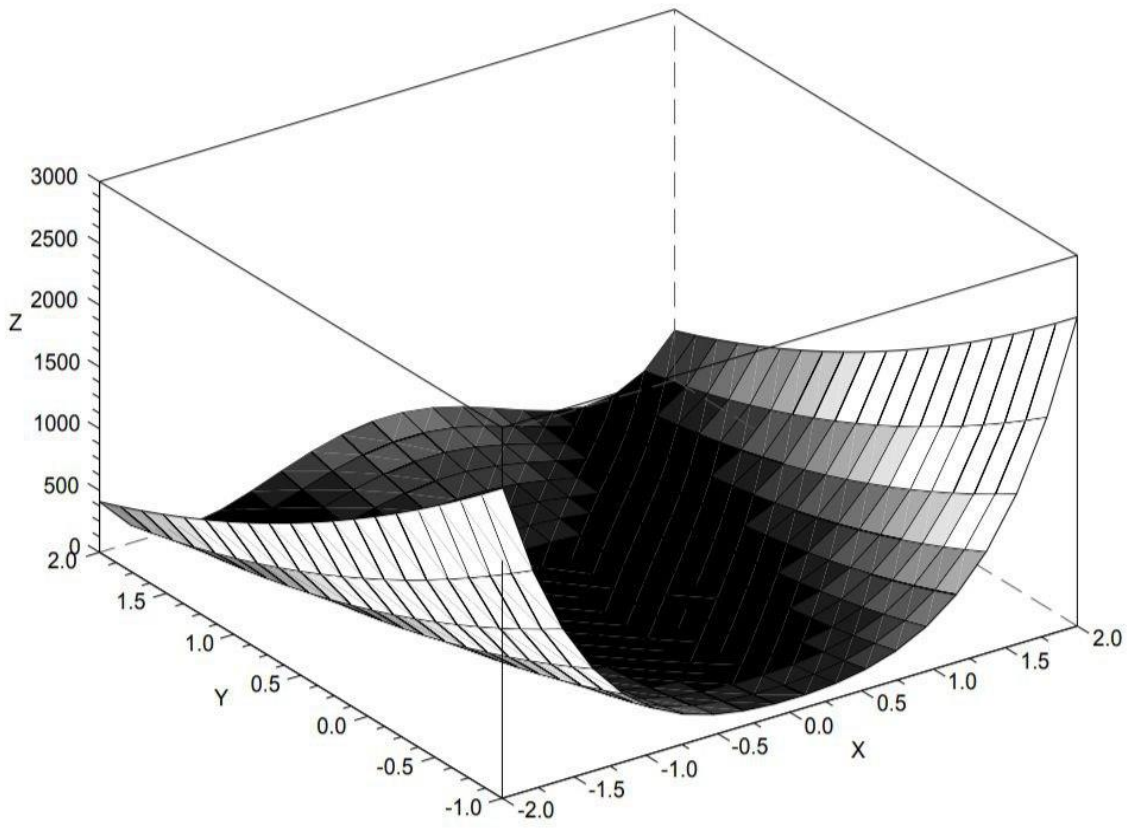

Figure: (3-1) Three dimensional plot of Rosenbrock's function [163].

3.12. Description of Rosenbrock's Method

The Rosenbrock technique is an optimization procedure that maximizes a function J of several variables T_1, i = 1 to n when the T_1's are subject to constraints

$$g_i (T_1, T_2, \ldots T_n) \leq T_i \leq h_i (T_1, T_2 \ldots T_n) \qquad i=1, 2, \ldots n \qquad (3\text{-}8)$$

$$g_{n+j} (T_1, T_2, \ldots T_n) \leq T_{n+j} (T_1, T_2 \ldots T_n) \qquad j=1, 2, \ldots p \qquad (3\text{-}9)$$

The search is conducted by progressing along vectors V_1 in the T's to extremize J, while guaranteeing compliance with the constraint equations.

The magnitude of the steps in each direction is autonomously decided by the algorithm, and the step directions are regularly modified. When adequate progress has been achieved[164]. Show in the Figure (3-2).

3.13. The Computer Code

The primary objective of this thesis is to develop computer models in FORTRAN to determine the optimal passively Q-switching operation within our constraints. The code developed in this study for the aforementioned objective has two components:

• The initial component is the Constrained Rosenbrock methodology.

• The subsequent component is a numerical simulation employing the Runge-Kutta-Fehlberg method to resolve rate equations, aimed at examining the dynamics of Cr: LiSAF passive Q-switching with Cr: YSO saturable absorber and calculating time-dependent variables.

The Constrained Rosenbrock method determines the optimal values for passively Q-switched systems, whereas the subsequent component computes the characteristics of the linked rate equations (objective functions). The computer software had three primary subroutines pertaining to the limitations. The first delineates the function to be restricted, the second delineates the lower bound of the constraints, and the third delineates the upper bound of the constraints.

The model's operation starts when the initial component receives input data, which is evaluated using the aforementioned subroutines to verify starting locations within restrictions. The first segment transmits the starting locations to the subsequent segment, which computes the goal functions.

Subsequent to this cycle, the proposed giant pulse form must be modified in each iteration based on the goal function's value; the parameters of the Constrained Rosenbrock approach, which pertain to the increase or decrease of the values, are analyzed to derive the giant pulse from the restrictions. This process is reiterated to attain the ideal result. The number of repetitions ranges

between 1000-3000 times. On $(\beta,\gamma_a,\gamma_c)$ were dealt with by step size of (0.001,0.1,1) respectively. The stopping condition for the program was set so that the difference between the objective function (equation (2-9)) and the number of input molecules was less than 10^{-3}. The model has the same flow chart that is shown in Figure (3-2).

The program is defined by the following attributes:

- Precision.
- Convenient utilization of the mode.

The input data may be categorized into two primary segments. The initial segment is as follows:

1. Nature of the optimal solution, whether it is a maximum or minimum.
2. Quantity of decision variables.
3. Step magnitude for each decision variable.

The second component consists of identical input data for the computer model.

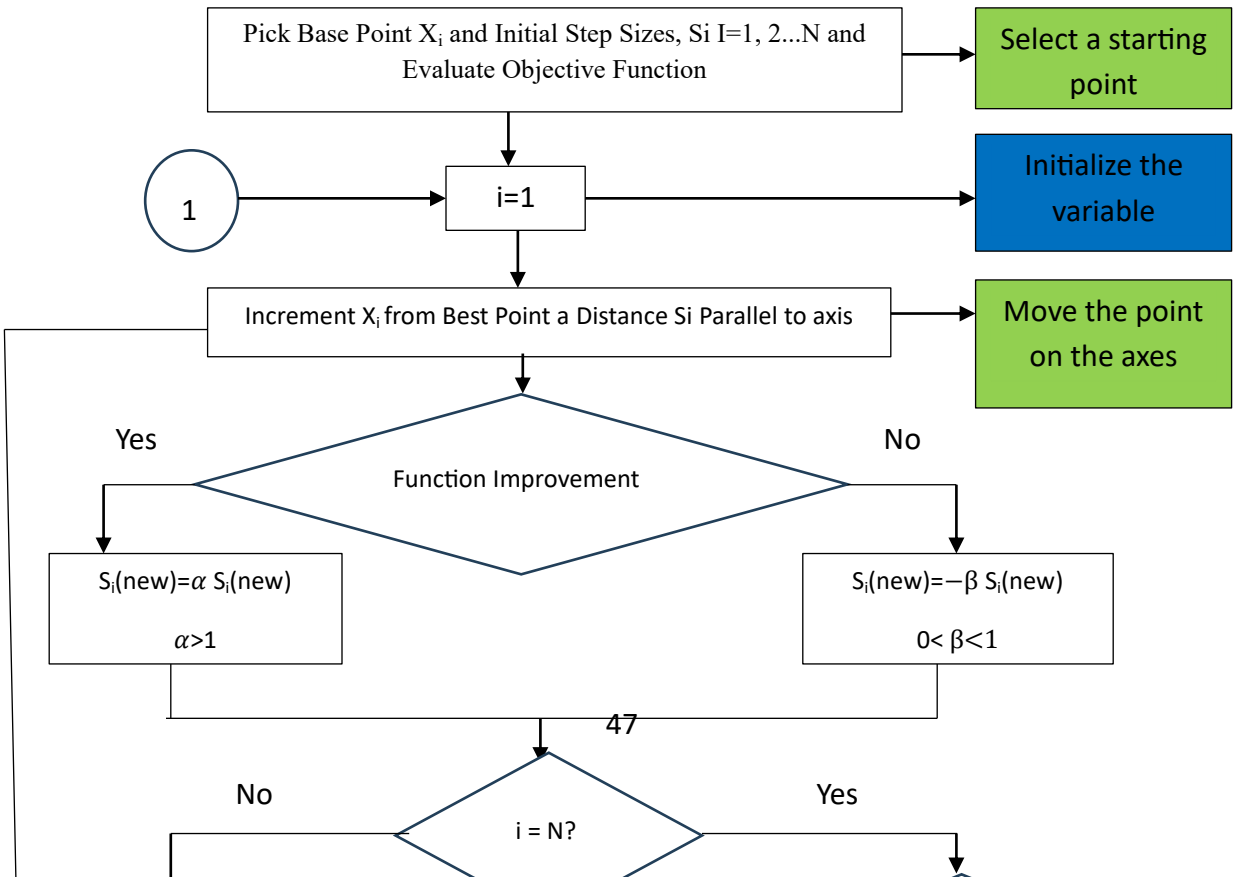

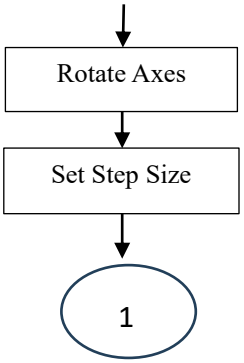

Figure: (3-2) Flow chart for the constrained Rosenbrock technique [159].

Chapter Four
Results and Discussion

4.1. Introduction

This chapter presents the results that came from the code and discusses them. The accuracy of the simulation program and the optimization program is listed, then the accuracy of the final code is also presented. Then, the optimal values for some rate equations parameters are found and discussed in more details which includes the optimal values of the absorption cross section of the first excited level to the absorption cross section of the ground level of the saturable absorber are, the optimal values of the decay rate of the saturable absorber and finally the optimal values of the decay rate of the photons, followed by the conclusions and future works.

4.2. Simulation Program Accuracy

A computer program was written to simulate the laser output pulse of a Cr: LiSAF laser with Cr: YSO as a saturable absorber. By numerically solving the rate equations (2-6, 2-7, 2-8, 2-9) using the Runge – Kutta – Fehlberg method. Table (4-1) represent the data that were fed to the program.

Table (4-1): The input data that used in the simulation program.

Parameter	Value[28]	Physical explanation
K_g	4.03×10^{-9} s^{-1}	The coupling coefficient between the stimulated photons and the active medium component.
K_a	1.52×10^{-8} s^{-1}	The coupling coefficient between photons and the saturable absorber molecules.
β	0.33	The excited state absorption cross-section to the ground state absorption cross-section of the saturable absorber molecules.
γ_a	1.43×10^{6} s^{-1}	The saturable absorber decay rate.
N_{ao}	2.30×10^{16}	Initial density of saturable absorber material.
γ_c	1.29×10^{8} s^{-1}	Photons losses inside the laser cavity.

γ_g	$1.49\times10^4\ s^{-1}$	The effective decay rate of the upper laser state.

The program's operation has been validated by achieving reference results[28]. The results summarized in table (4-2).

Table (4-2): Comparison of simulation results extracted from the program and published results.

Parameter	simulation results	Published value[165]	Absolute error	Relative error
Pulse duration	35.85ns	35ns	0.85ns	2.4%
Pulse energy	4.27mJ	4.3 mJ	0.03 mJ	0.7%

The differences between the calculated and published values are very small, which indicates that the program is very accurate. This is evidence of the efficiency of the numerical method used and the accuracy of entering the physical parameters.

4.3. Optimization Program Accuracy

A sample problem has been selected to execute the program, wherein the objective function of two variables is inputted ($F(X) = 3803.84 + 138.08 * x_1 + 232.92 * x_2 – 123.08 * x_1^2 – 203.64 * x_2^2 - 182.25 * x_1 * x_2$). The computed values of the variables x_1 and x_2 in maximization mode correspond to those published in the[159].

4.4. The Code Accuracy

The Constrained Rosenbrock optimization technique was used to determine the optimal operating conditions for the passively Q-switching mode laser system by linking the simulation program with the optimization program, so they became one code. To validate the correctness of the program’s operation, the calculated results

were compared with those reported in the published literature, as shown in Table (4-3).

Table (4-3): Comparison between code results and published results.

Parameter	Values calculated in the program	Published value[28]	Absolute error	Relative error
β	0.3001	0.33	0.0299	0.09%
γ_a	1430009	1.43×10^{6}	0.000009	0.06%
γ_c	129000320	1.29×10^{8}	0.0000024	2.4%

The reason for the slight difference between the calculated and published results could be due the physical and mathematical approximations of the rate equations.

4.5. Finding the Optimum Values for Some Rate Equations Parameters

The Constrained Rosenbrock optimization Technique was used to find the optimal values for some parameters of the rate equations (2-6, 2-7, 2-8, 2-9) that solved numerically when the number of saturable absorber molecules changed from 2.3×10^{16} to 7.3×10^{16}. The maximization option for the objective functions (the rate equations in our case) was used to get the values of β, γ_a,γ_c as shown in table (4-4).

Table (4-4): Optimum values of β, γa, γc at different molecules numbers.

Molecule Numbers $x10^{16}$ (mol/m^2)	Optimum β values	Optimum γ_a values (Sec^{-1})	Optimum γ_c values (Sec^{-1})	Pulse Duration (nsec)	Pulse Energy (mJ)	Pulse power (Watt)
2.3	0.3001	1430009	129000320	35.1	4.19	119429.35
3.3	0.3002	1349229	129000321	19.39	8.36	431236.91

4.3	0.3005	1429994	129000456	16.41	14.74	898024.86
5.3	0.3382	1200081	129559971	15.77	25.34	1637520.66
6.3	0.3580	1200083	127782046	12.46	25.11	2014763.57
7.3	0.4084	1200020	124607628	9.76	48.76	4993090.63

We notice from the values in Table (4-4) that the value of(β)increases with the increase in the number of molecules, while the values of (γ_a, γ_c) decrease with the increase in the number of molecules. We notice that there is a sudden increase in the value of γ_a over the number of molecules, 4.3 x 10^{16}, It is believed that this increase is due to the algorithm being given an unstable initial value for γ_a, which affected the objective function and gave a non-local result. The significant increase in pulse power indicates the numerical tuning used to improve the optimal operating conditions, as the chosen values of parameters ($\beta, \gamma_a, \gamma_{c)}$ contributed to obtaining a pulse with high energy and short duration, which is the primary goal in designing a Q_switching laser.

4.6. Optimum Values of Absorption cross section of the first excited state to the absorption cross section of the ground state of the saturable absorber material (β)

The absorption efficacy of a saturable absorber depends on many factors: the number of energy levels participating in absorption (i-The value of the absorption cross-section of those levels. ii- The lifetime of the level as this affects the number and time of the presence of molecules in it. iii-The availability of another level higher than it that achieves the quantum nature of absorption). The molecular distribution across these levels, and the absorption cross-sections σ_a. This was observed from the findings obtained.

An augmentation in the quantity of molecules results in an elevation in the value of (β). See Figure (4-1). Where β is the ratio of the absorption cross-section for the first excited state of the absorbing material to that of its ground state, it is expressed by the following relationship: β= $K_{a\ excl}/K_{ag}$.

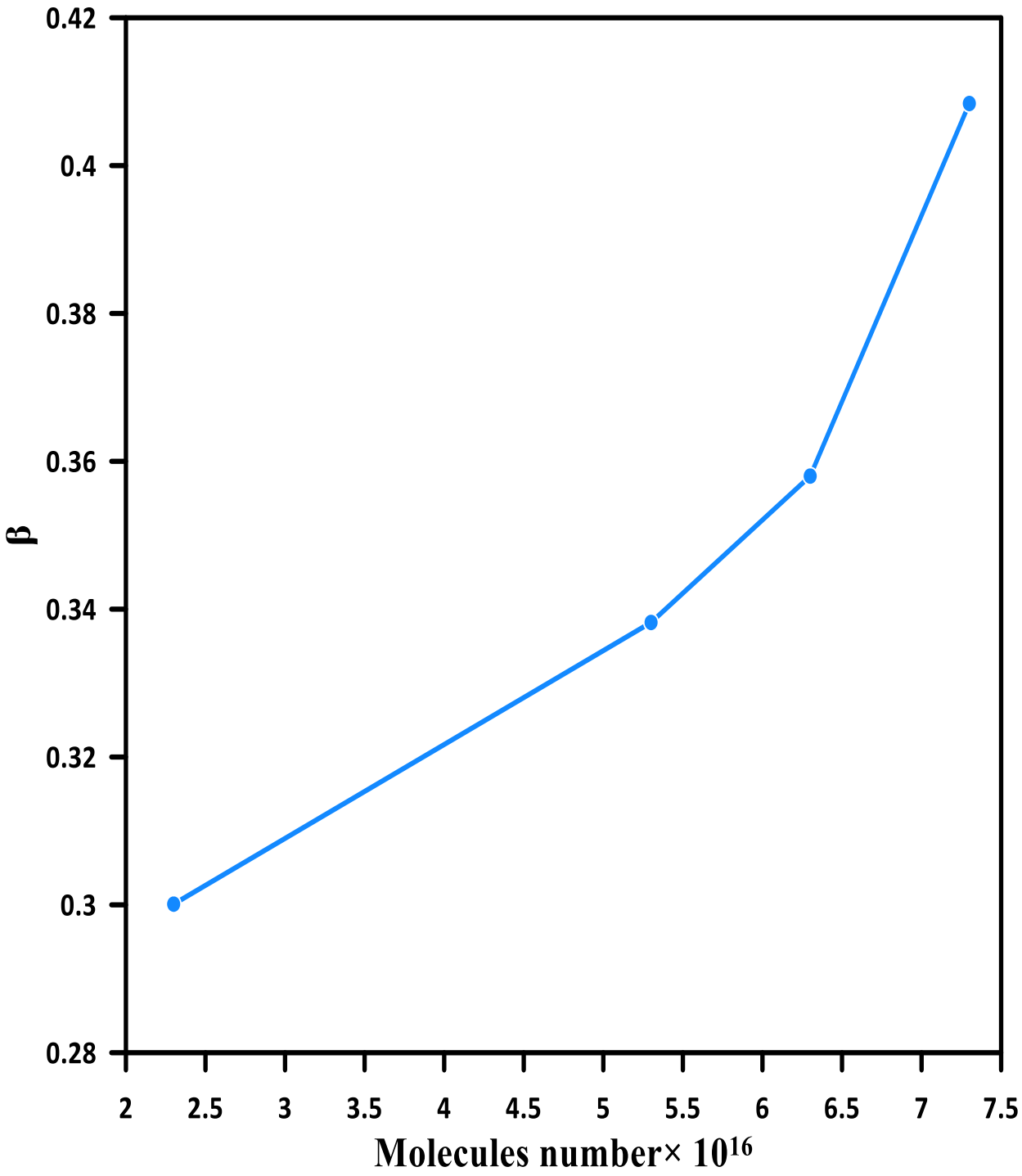

Figure: (4-1) β as a function of molecules number of saturable absorber.

This enhancement in the absorption capacity of the first excited state leads to an overt increase in absorption efficiency of the saturable absorber material. The observed improvement, associated with the increase in the β parameter; induces

substantial photon losses within the laser resonator. Consequently, this results in a higher population inversion in the active medium, which in turn enhances the pulse energy, as demonstrated in Figure (4-2).

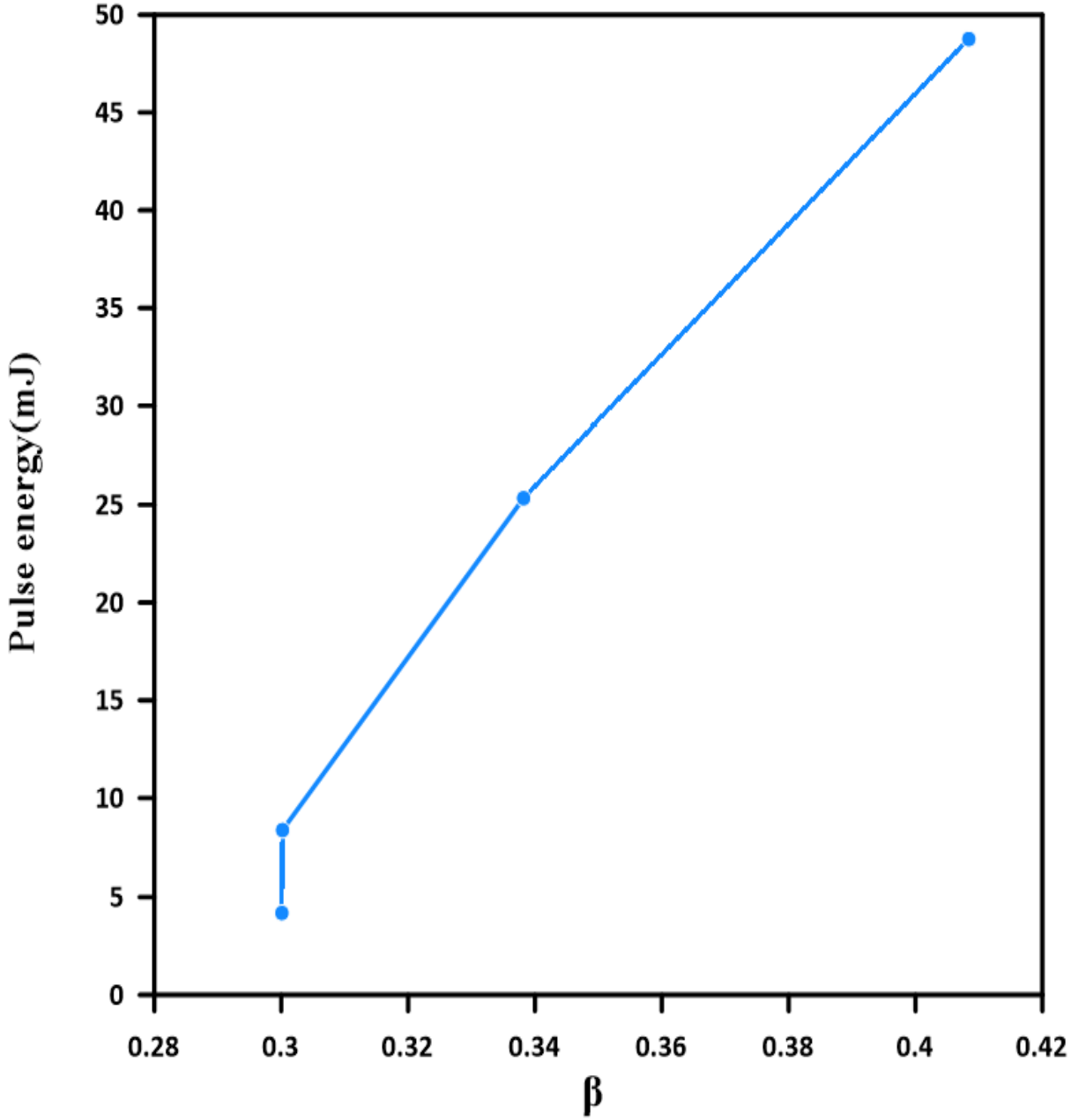

Figure: (4-2) β as a function of pulse energy.

Conversely, the pulse duration decreases with increasing value of β, show in Figure (4-3).

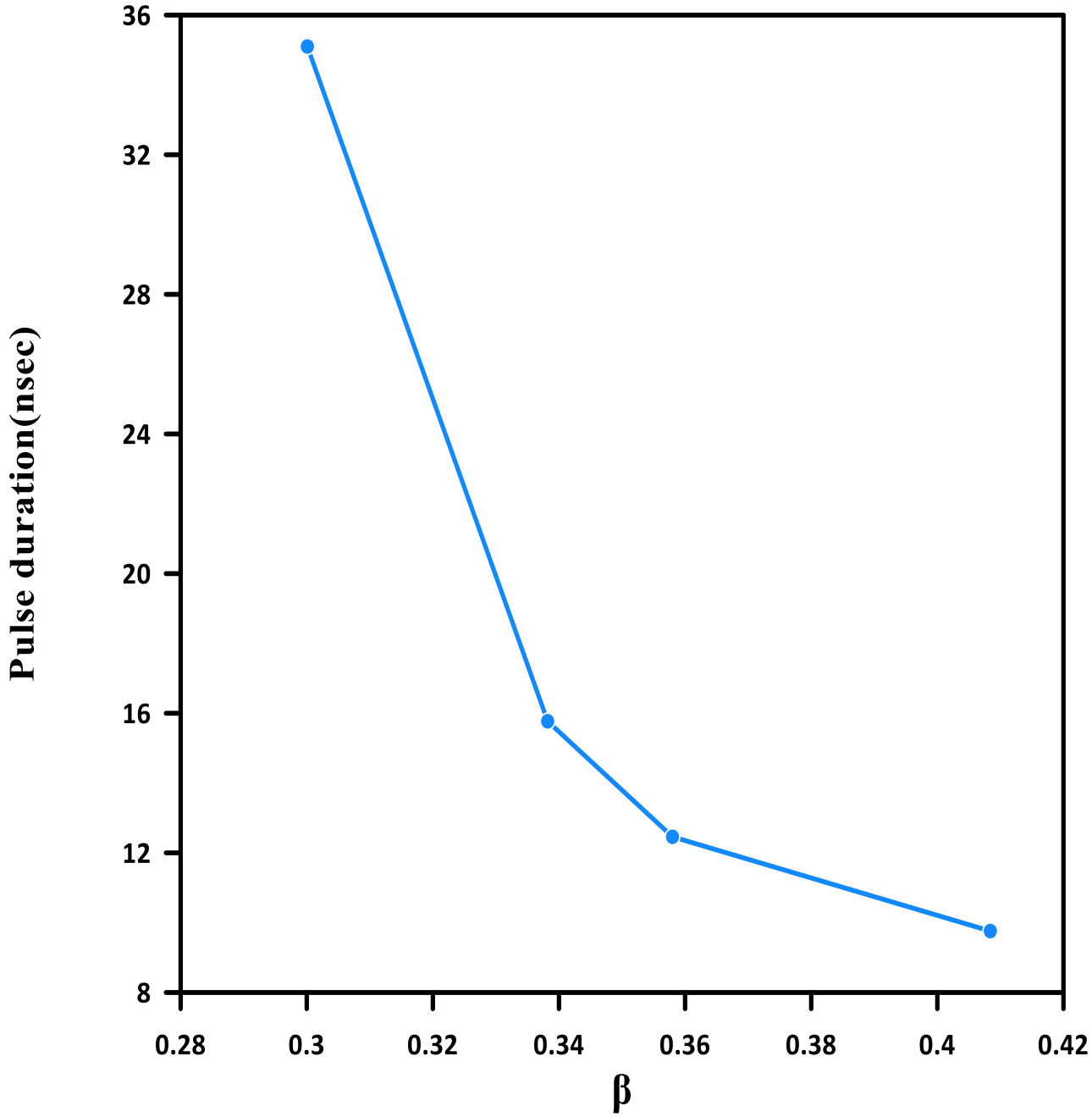

Figure: (4-3) β as a function of pulse duration.

4.7. Optimum Values of Relaxation Rate of the saturable absorber material(γ_a)

The $\gamma_a$values diminish as the number of saturable absorber molecules (ni) increases until a certain value of (ni) (5.5×10^{16}) is attained, beyond which the

variation becomes insignificant and may be regarded as constant at this level. As shown in Figure (4-4).

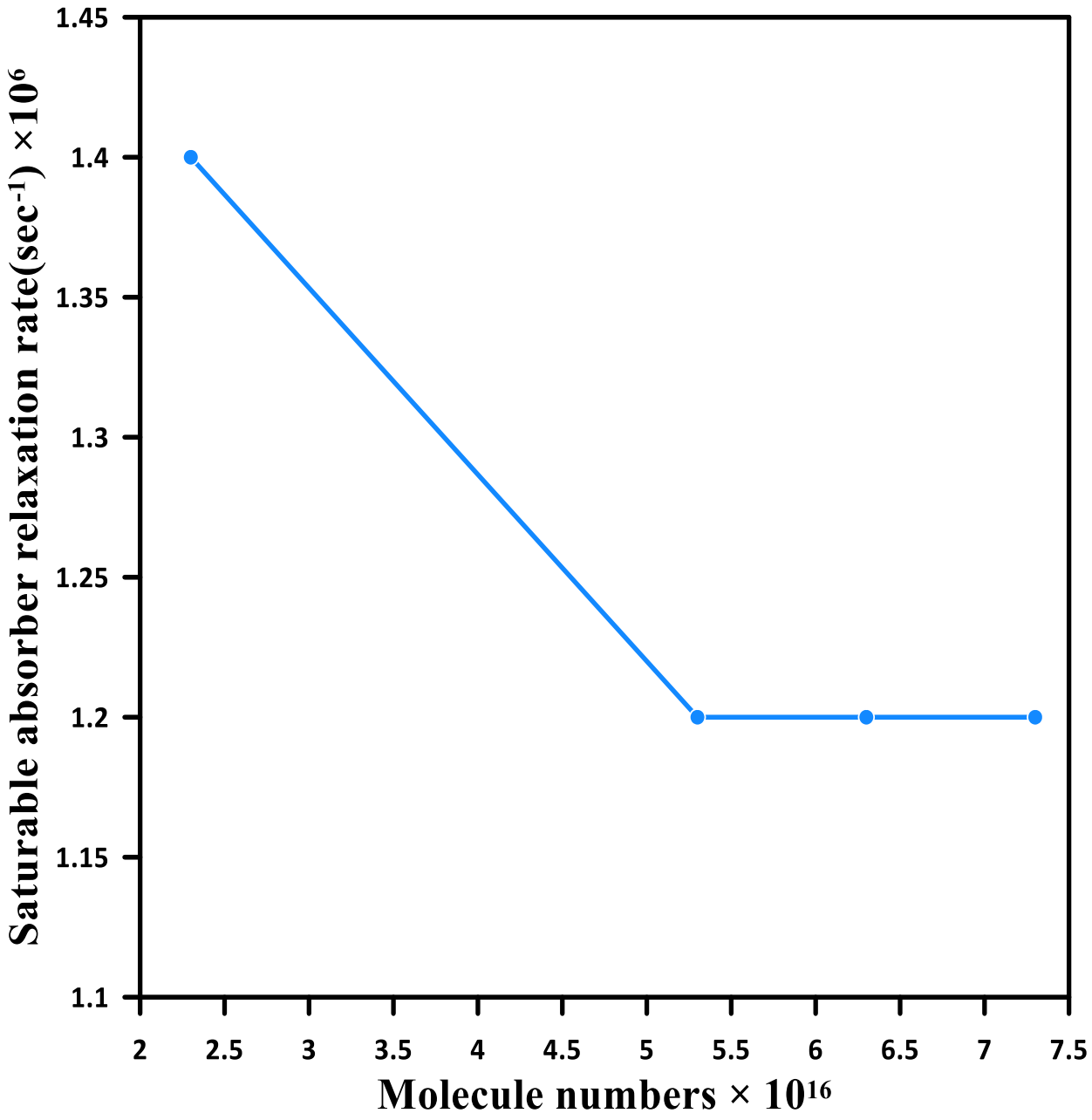

Figure: (4-4) The profile of relaxation rate as a function of Cr: YSO molecule numbers.

The number of molecules at each energy level is governed by the Boltzmann distribution. The increase of Cr: YSO molecules in the ground state will lead to a

little increase in the number of molecules in the first excited state. Therefore, this will not improve the intersystem crossing rate, a factor that affects the elongation of relaxation time and, subsequently, recovery time, which is linked to pulse duration. The figures (4-5) and (4-6) illustrate the effect of relaxation rate on pulse energy and duration.

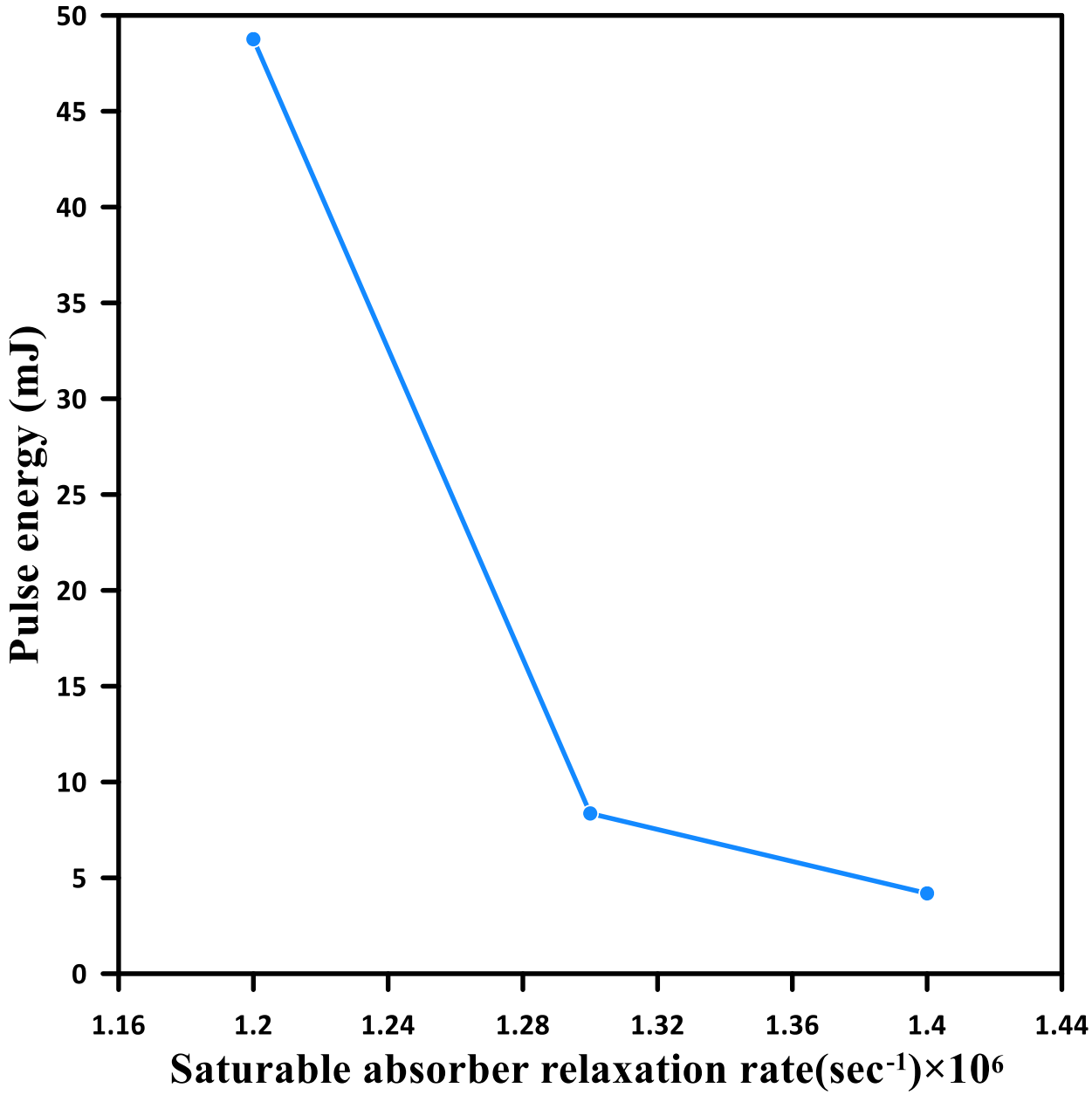

Figure: (4-5) Relaxation rate as a function of pulse energy.

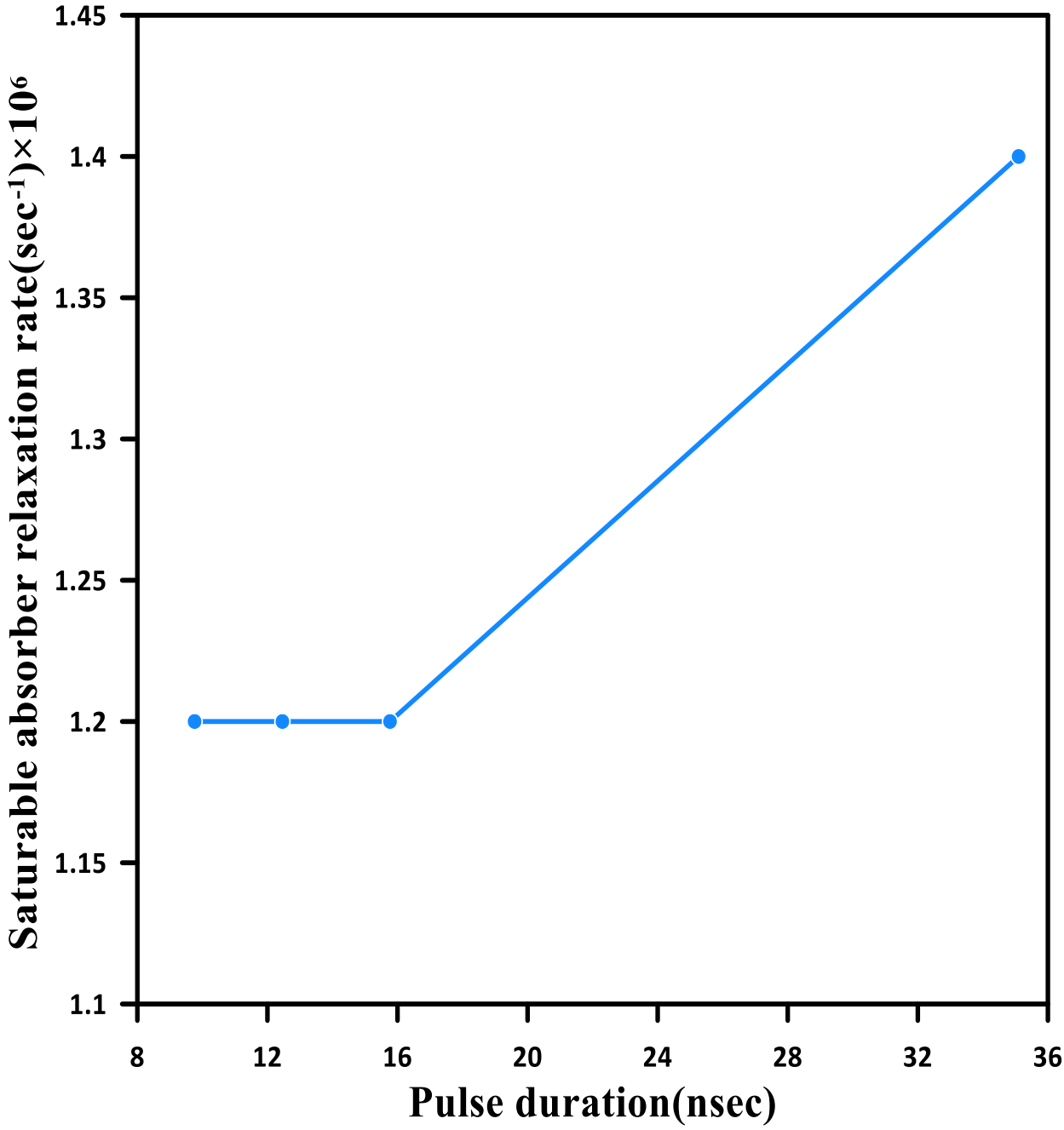

Figure: (4-6) Relaxation rate as a function of pulse duration.

4.8. Optimum Values of Average Cavity Photons Decay Rate (γ_c)

When photons coming out of the active medium due to pumping fall on the saturable absorber, they are absorbed by the molecules of the saturable absorber. This leads to

the excitation of the ground state molecules and their movement to the higher levels.

Therefore, we notice in Fig. (4-7) a decrease in the ground state molecules with time.

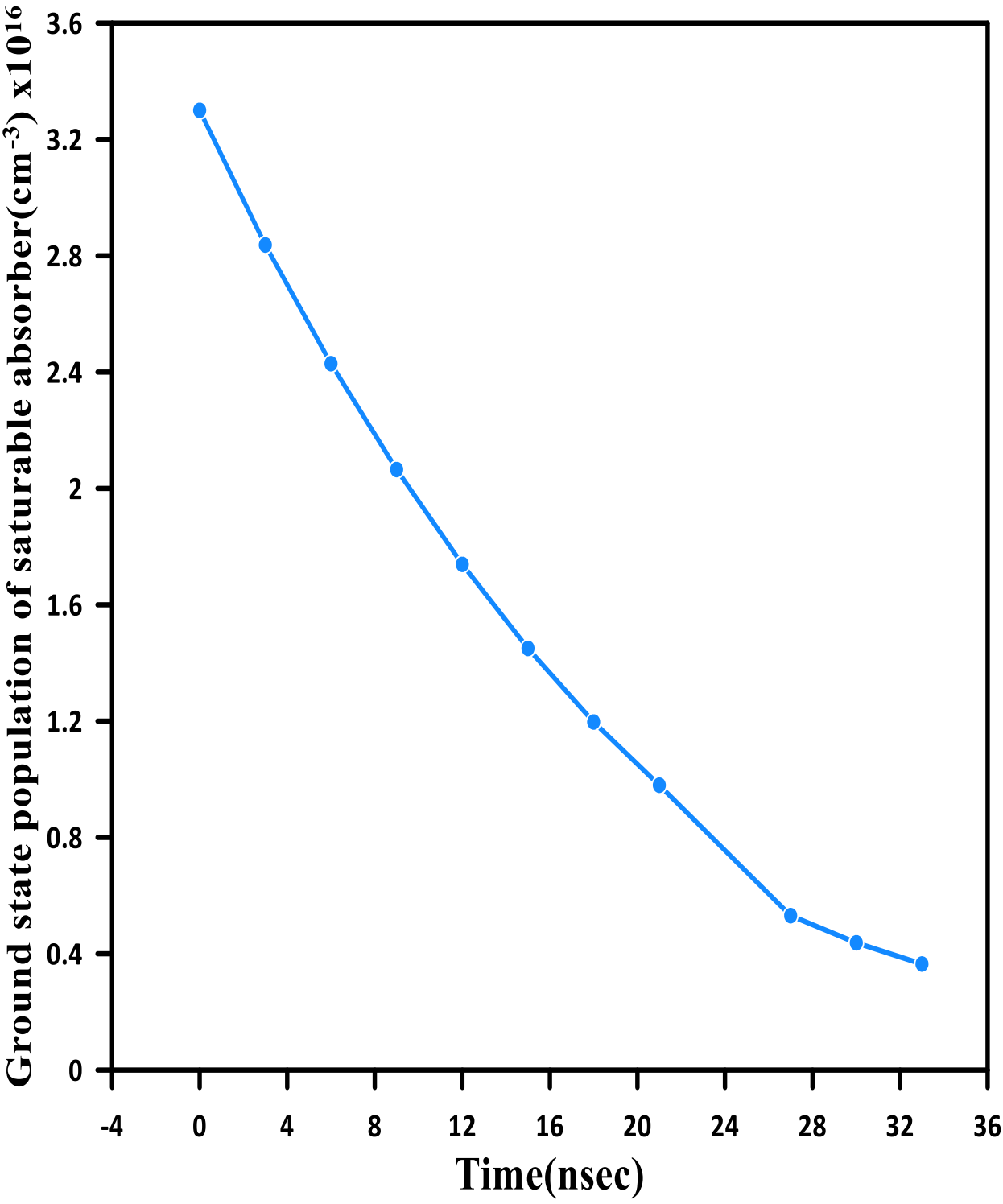

Figure: (4-7) Ground state population of saturable absorber as a function of time.

The transfer of molecules to the first excited state leads to an increase in the number of molecules in this state with time. Figure (4-8) illustrates this.

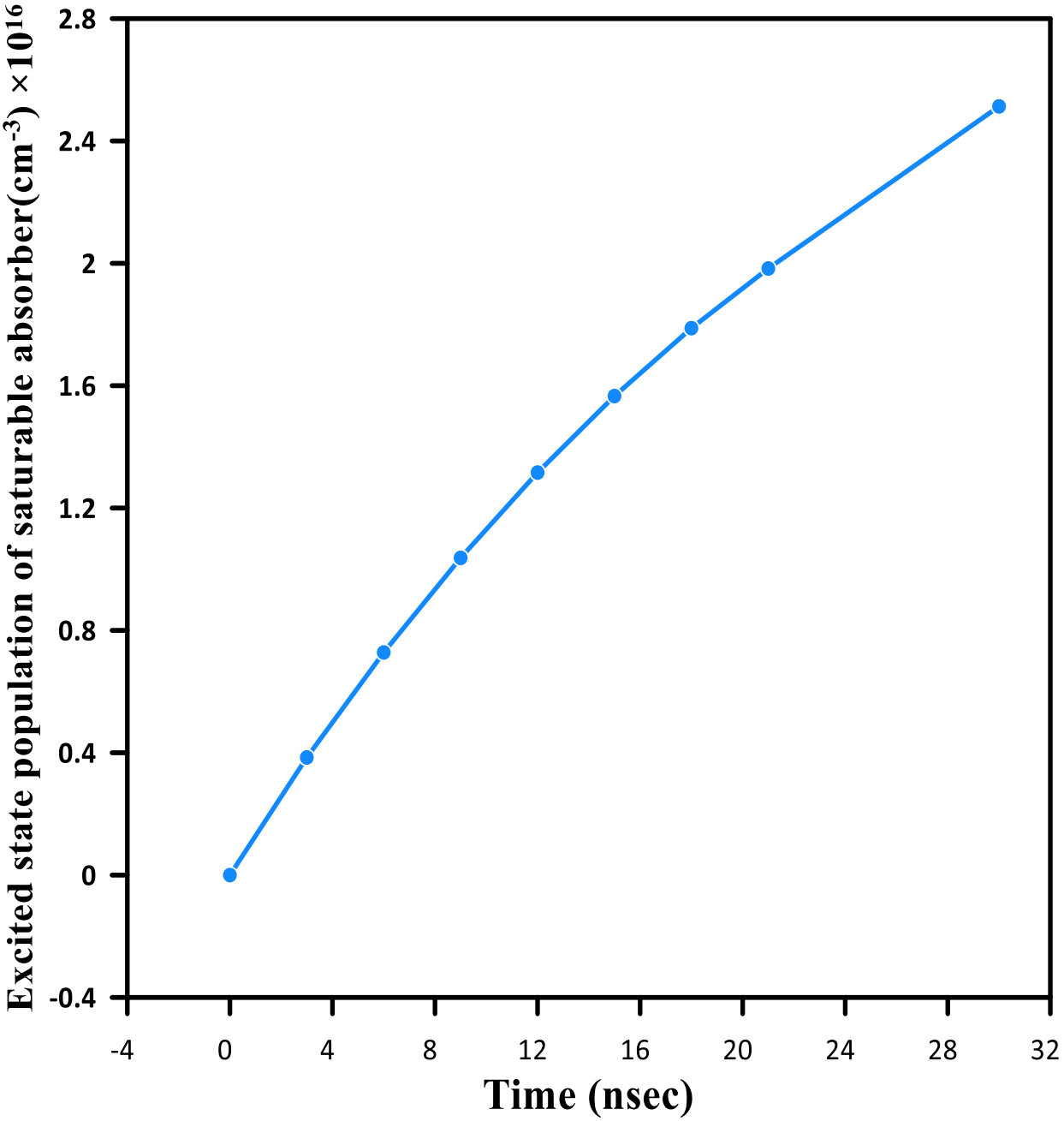

Figure: (4-8) Excited state population of saturable absorber as a function of time.

This absorption of photons leads to photon losses inside the resonator (γ_c), as we notice in Figure (4-9) that the highest values of photon losses are at the initial values of the molecules, then they begin to decrease until they reach a certain value,

then they become negligible due to the saturable absorber material reaching the saturation state.

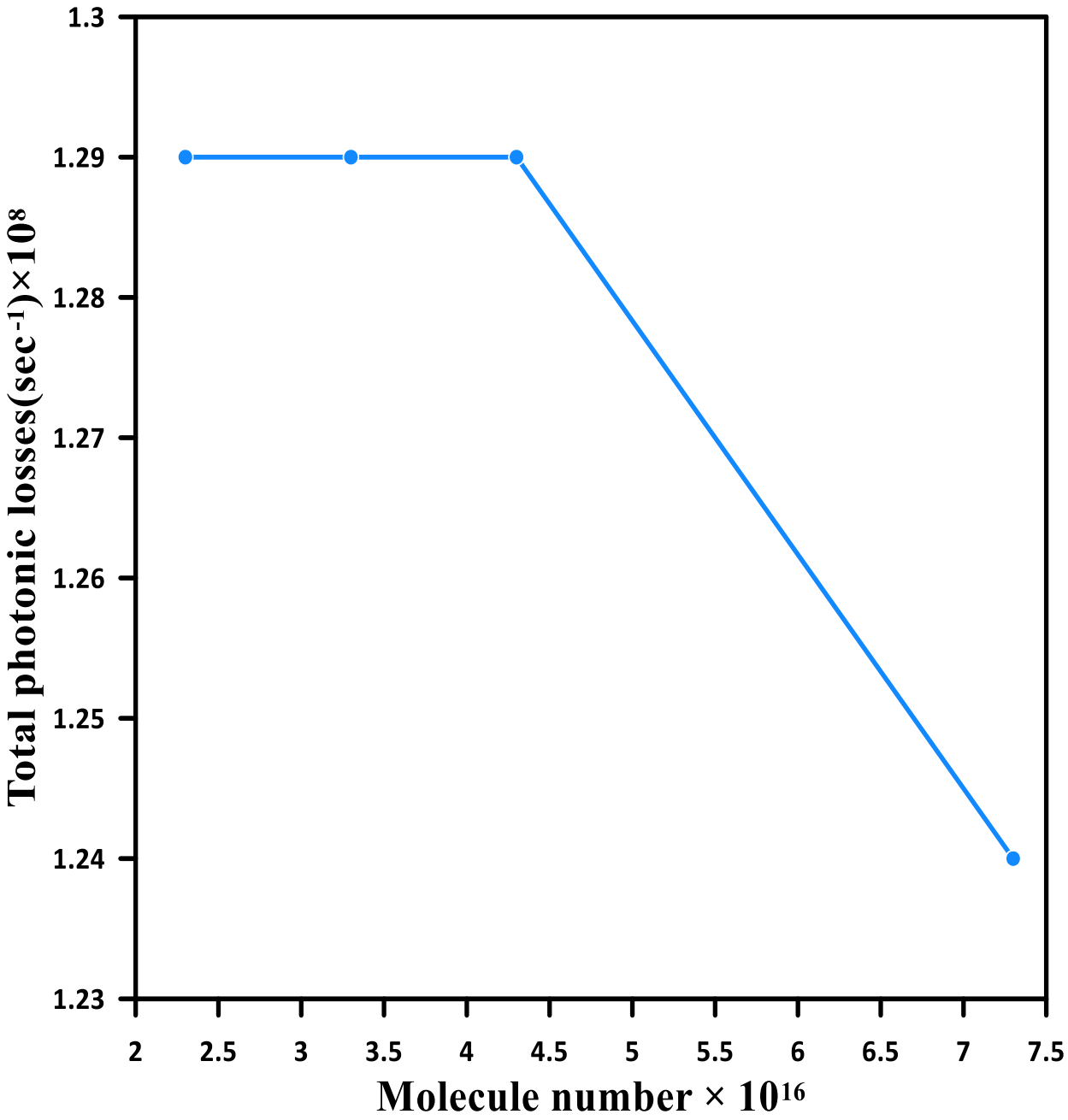

Figure: (4-9) The profile of total photonic losses as a function of Cr: YSO molecules number.

High photons losses inside the resonator affect the inverse population inside the active medium, leading to a high initial inverse population inside the active medium, then it drops dramatically when the giant pulse is launched. as shown in Figure (4-10).

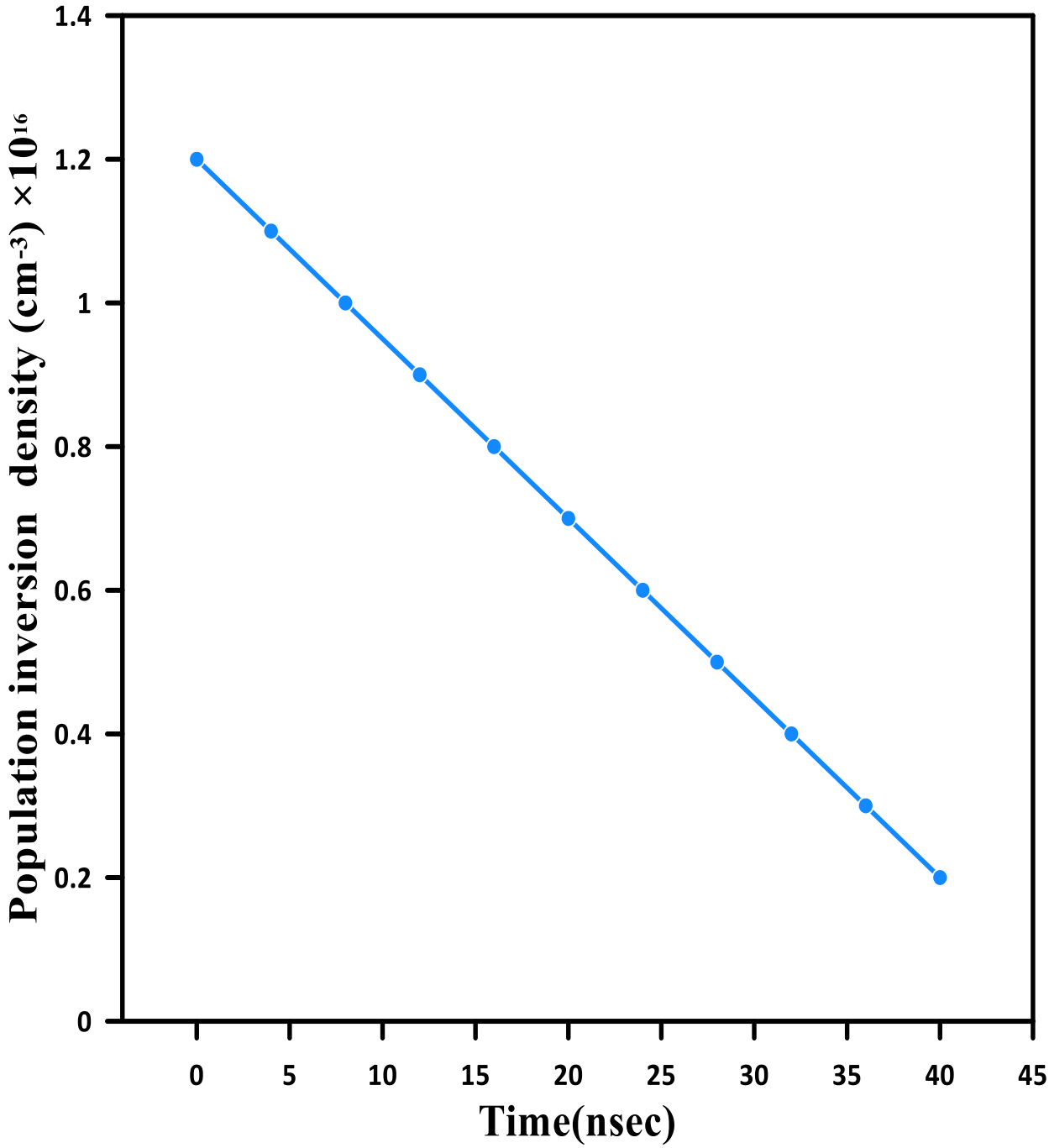

Figure: (4-10) The time variation of final population inversion density.

That is, there is a high of energy storage within the active medium through which a high-energy, short-duration pulse is obtained, which is released when the material reaches a state of saturation. See Figure (4-11).

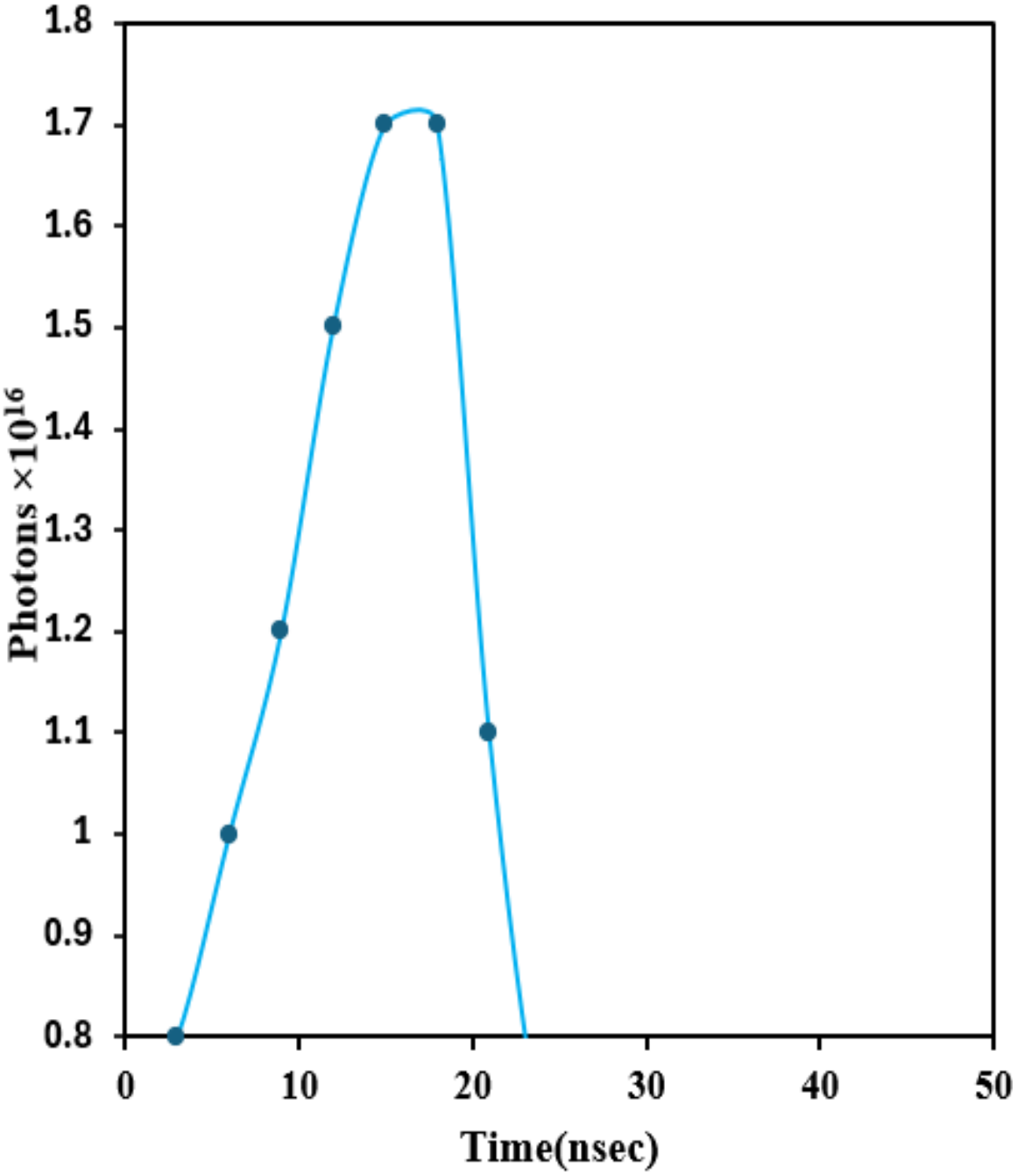

Figure: (4-11) The stimulated photons profile.

4.9. Conclusions

The study reports the following conclusions:

- By applying the constrained Rosenbrock Optimization technique to a Cr: LiSAF laser passively Q-switched by a Cr: YSO saturable absorber, it was observed that the value of the parameter β increases with increase in the number of Cr: YSO molecules. This indicates an enhancement in the absorbers capability to capture photons, which results in increased pulse energy and power, accompanied by a reduction in pulse duration.
- The relaxation time (τ_a) of the Cr: YSO saturable absorber, was found to be directly proportional to the number of Cr: YSO molecules, confirming the sensitivity of this parameter to the absorbers molecular.
- Both the relaxation rate (γ_a) of the Cr: YSO and photons losses rate (γ_c) decrease as the number of Cr: YSO molecules increases, up to a certain threshold beyond which further variation becomes negligible. This behavior contributes to improved pulse energy and shorter pulse duration.
- The overall results confirm that the constraint Rosenbrock optimization technique is highly effective in determining the optimal values key decision variables related to the performance of the Cr: LiSAF laser passively Q-switched by Cr: YSO saturable absorber. The method is particularly distinguished by its ability to handle constraints on parameters ($\beta, \gamma_a, \gamma_c$), there by yielding accurate and well- balanced solutions accurate solutions for achieving optimal laser operation conditions.

4.10. Future Works

1. Applying the optimization techniques to developed theoretical model that takes into account the absorption occurring at the fifth energy level, with a comparison of the obtained results to conventional two-level.
2. Calculating the coupling coefficients of the active medium and the saturable absorber in different system using optimization techniques, with aim or enlacing laser performance and achieving optimal pulse characteristics.
3. Determining the optimal geometry shape and volume of both the active medium and the saturable absorber to obtain improved pulse characteristics in terms of energy pulse duration, and repetition rate, using advanced numerical simulation techniques.
4. Studying of the effects of environmental factors, such as temperature and humidity on the performance of the saturable absorber through experimental measurements and theoretical modeling, along with evaluating the absorber's stability under varying operating condition.

References

[1] C. C. Marouchos, *The switching function: analysis of power electronic circuits* vol. 17: IET, 2006.

[2] R. Agrahari, S. K. Ghosh, and S. Bhattacharyya, "Optical Switches," *Optical Switching: Device Technology and Applications in Networks,* pp. 13-30, 2022.

[3] P. De Dobbelaere, K. Falta, S. Gloeckner, and S. Patra, "Digital MEMS for optical switching," *IEEE Communications magazine,* vol. 40, pp. 88-95, 2002.

[4] V. Sasikala and K. Chitra, "All optical switching and associated technologies: a review," *Journal of Optics,* vol. 47, pp. 307-317, 2018.

[5] X. Ma and G.-S. Kuo, "Optical switching technology comparison: optical MEMS vs. other technologies," *IEEE communications magazine,* vol. 41, pp. S16-S23, 2003.

[6] G. I. Papadimitriou, C. Papazoglou, A. S. Pomportsis, and Tutorial), "Optical switching: switch fabrics, techniques, and architectures," *Journal of lightwave technology,* vol. 21, p. 384, 2003.

[7] G. Coppola, L. Sirleto, I. Rendina, and M. Iodice, "Advance in thermo-optical switches: principles, materials, design, and device structure," *Optical Engineering,* vol. 50, pp. 071112-071112-14, 2011.

[8] T. Goh, "Recent advances in large-scale silica-based thermo-optic switches," *Optical Switching and Optical Interconnection,* vol. 4582, pp. 49-56, 2001.

[9] G. Cocorullo, F. Della Corte, and I. Rendina, "Temperature dependence of the thermo-optic coefficient in crystalline silicon between room temperature and 550 K at the wavelength of 1523 nm," *Applied physics letters,* vol. 74, pp. 3338-3340, 1999.

[10] K. THAKULSUKANANT, "Mems technology for optical switching," *Walailak Journal of Science and Technology (WJST),* vol. 10, pp. 9-18, 2013.

[11] T.-W. Yeow, K. E. Law, and A. Goldenberg, "MEMS optical switches," *IEEE Communications magazine,* vol. 39, pp. 158-163, 2001.

[12] C. V. Garcìa, I. P. Garcilópez, P. C. Lallana, B. Vinouze, and B. Fracasso, "Liquid crystal optical switches," in *Optical Switches*, ed: Elsevier, 2010, pp. 206-240.

[13] J.-C. Chiao, "Liquid-crystal optical switches," in *Photonics in Switching*, 2001, p. JWB2.

[14] D.-K. Yang and S.-T. Wu, *Fundamentals of liquid crystal devices*: John Wiley & Sons, 2014.

[15] M. Y. Kariduraganavar, R. V. Doddamani, B. Waddar, and S. R. Parne, "Nonlinear optical responsive molecular switches," *Nonlinear Optics-From Solitons to Similaritons,* p. 187, 2021.

[16] P. Beaujean, F. Bondu, A. Plaquet, J. Garcia-Amoros, J. Cusido, F. M. Raymo*, et al.*, "Oxazines: a new class of second-order nonlinear optical switches," *Journal of the American Chemical Society,* vol. 138, pp. 5052-5062, 2016.

[17] H. Chen, J. Li, Z. Shang, G. Wang, Z. Zhang, Z. Zhao*, et al.*, "Inverse-designed integrated nonlinear optical switches," *Laser & Photonics Reviews,* vol. 16, p. 2200254, 2022.

[18] S. R. Marder, J. E. Sohn, and G. D. Stucky, *Materials for nonlinear optics: chemical perspectives*: ACS Publications, 1991.

[19] N. Peyghambarian, S. W. Koch, and A. Mysyrowicz, *Introduction to semiconductor optics*: Prentice-Hall, Inc., 1993.

[20] R. V. Doddamani, R. G. Tasaganva, S. R. Inamdar, and M. Y. Kariduraganavar, "Synthesis of chromophores and polyimides with a green chemistry approach for second-order nonlinear optical applications," *Polymers for Advanced Technologies,* vol. 29, pp. 2091-2102, 2018.

[21] X.-S. Xing, R.-J. Sa, P.-X. Li, N.-N. Zhang, Z.-Y. Zhou, B.-W. Liu*, et al.*, "Second-order nonlinear optical switching with a record-high contrast for a photochromic and thermochromic bistable crystal," *Chemical Science,* vol. 8, pp. 7751-7757, 2017.

[22] J. Wu, J. Luo, and A. K.-Y. Jen, "High-performance organic second-and third-order nonlinear optical materials for ultrafast information processing," *Journal of Materials Chemistry C,* vol. 8, pp. 15009-15026, 2020.

[23] S. Aleksic, M. Fiorani, and M. Casoni, "Adaptive hybrid optical switching: performance and energy efficiency," *Journal of High Speed Networks,* vol. 19, pp. 85-98, 2013.

[24] M. Fiorani, S. Aleksic, and M. Casoni, "Hybrid optical switching for data center networks," *Journal of Electrical and Computer Engineering,* vol. 2014, p. 139213, 2014.

[25] Y.-K. Kuo, J. Chang, and H. Chen, "Broadband Cr: YSO solid state saturable absorber for ruby, alexandrite, and Cr: LiCAF lasers: numerical study on passive Q-switching performance," in *Optoelectronic Materials and Devices II*, 2000, pp. 587-594.

[26] Y.-K. K. Y.-K. Kuo and J.-Y. C. J.-Y. Chang, "Numerical study on passive Q-switching of tunable Cr: LiCAF laser with Cr: YSO solid state saturable absorber," *Japanese Journal of Applied Physics,* vol. 40, p. 5949, 2001.

[27] C.-K. Chang, J. Chang, and Y.-K. Kuo, "Optical Performance of Cr: YSO Q-switched Cr: LiCAF and Cr: LiSAF Lasers," in *High-Power Lasers and Applications II*, 2002, pp. 498-509.

[28] H.-F. Chen, S.-W. Hsieh, and Y.-K. Kuo, "Simulation of tunable Cr: YSO Q-switched Cr: LiSAF laser," in *High-Power Lasers and Applications III*, 2005, pp. 488-498.

[29] S. N. A.-W. M. Mutter, "The study of the Cr4+: Y2SiO5 crystal coupling coefficients as a solid Q-switch for the chromic solid-state lasers," *Journal of Basrah Researches (Sciences),* vol. 33, 2007.

[30] H. N. Van, H. N. Dinh, Q. N. Khoa, T. D. Duy, and H. N. Dai, "Characteristics of Diode End-Pumped Passively Q-Switched Solid-State Cr 3+: LiSAF Laser," *CMST,* pp. 27-31, 2010.

[31] N. Van Hao, P. H. Minh, P. Van Duong, and N. Dai Hung, "Numerical Investigations of Laser Diode End-pumped Solid-state Cr\(^{3+}\): LiSAF Lasers Passively Q-switched with Cr\(^{4+}\): YSO Crystal," *Communications in Physics,* vol. 24, pp. 71–84-71–84, 2014.

[32] A.-K. M. Salih, "Influence of Absorption cross section of saturable absorber on Passive Q-switching laser pulse characteristics," *University of Thi-Qar Journal of Science,* vol. 4, pp. 99-104, 2014.

[33] K. Shimoda, *Introduction to laser physics* vol. 44: Springer, 2013.

[34] W. T. Silfvast, *Laser fundamentals*: Cambridge university press, 2004.

[35] S. Bjurshagen, "Diode-pumped Nd: YAG lasers for generation of blue light by frequency doubling," Fysik, 2004.

[36] X. Jiang, A. V. Kuklin, A. Baev, Y. Ge, H. Ågren, H. Zhang*, et al.*, "Two-dimensional MXenes: From morphological to optical, electric, and magnetic properties and applications," *Physics Reports,* vol. 848, pp. 1-58, 2020.

[37] H. Ahmad, H. S. Albaqawi, N. Yusoff, L. Bayang, M. Z. B. A. Kadir, and C. W. Yi, "Tunable passively Q-switched erbium-doped fiber laser based on Ti3C2Tx MXene as saturable absorber," *Optical Fiber Technology,* vol. 58, p. 102287, 2020.

[38] H. N. Y. Nguyen and W. Steenbergen, "Feasibility of identifying reflection artifacts in photoacoustic imaging using two-wavelength excitation," *Biomedical optics express,* vol. 11, pp. 5745-5759, 2020.

[39] M. Aoki and H. Iwai, "Dual-wavelength locking technique for coherent 2-μm differential absorption lidar applications," *Applied Optics,* vol. 60, pp. 4259-4265, 2021.

[40] Y. Wang, A. Chen, Q. Wang, D. Zhang, S. Li, Y. Jiang*, et al.*, "Study of signal enhancement in collinear femtosecond-nanosecond double-pulse laser-induced breakdown spectroscopy," *Optics & Laser Technology,* vol. 122, p. 105887, 2020.

[41] J. Wang, L. Xie, Y. Wang, Y. Lan, P. Wu, J. Lv*, et al.*, "High-damage vanadium pentoxide film saturable absorber for sub-nanosecond Nd: YAG lasers," *Infrared Physics & Technology,* vol. 129, p. 104580, 2023.

[42] K. Zeng, X. Wu, F. Jiang, J. Zhang, J. Kong, J. Shen*, et al.*, "Experimental research on micro hole drilling of polycrystalline Nd: YAG," *Ceramics International,* vol. 48, pp. 9658-9666, 2022.

[43] Z.-Y. Zhao, Z.-T. Cai, C.-M. Zhao, and J. Zhang, "Solar-pumped 1061-/1064-nm dual-wavelength Nd: YAG monolithic laser," *Optical Engineering,* vol. 62, pp. 036103-036103, 2023.

[44] C.-Y. Kao and F. Santosa, "Maximization of the quality factor of an optical resonator," *Wave motion,* vol. 45, pp. 412-427, 2008.

[45] M. C. Teich and B. Saleh, *Fundamentals of photonics* vol. 2: Wiley New Jersey, 2007.

[46] C. Perrière, R. Boulesteix, A. Maitre, B. Forestier, A. Jalocha, and A. Brenier, "Study of dopant distribution in Cr4+: YAG transparent ceramics and its use as passively Q-switching media in Nd: YAG laser delivering 38 mJ per pulse," *Optical Materials: X,* vol. 12, p. 100107, 2021.

[47] U. Keller and R. Paschotta, *Ultrafast lasers*: Springer, 2021.

[48] Y.-F. Chen and S. Tsai, "Simultaneous Q-switching and mode-locking in a diode-pumped Nd: YVO/sub 4/-Cr/sup 4+: YAG laser," *IEEE journal of quantum electronics,* vol. 37, pp. 580-586, 2001.

[49] F. Z. Jasim, "Study of Q-switching Effects on Nd:YAG Laser performance," College of Engineering, Al-Nahrain University,, 2004.

[50] R. Paschotta, *Encyclopedia of laser physics and technology* vol. 1: Wiley Online Library, 2008.

[51] Y. Wang and C.-Q. Xu, "Actively Q-switched fiber lasers: Switching dynamics and nonlinear processes," *Progress in Quantum Electronics,* vol. 31, pp. 131-216, 2007.

[52] A. Bizjak, K. Nemeš, and J. Možina, "Rotating-mirror Q-switched Er: YAG laser for optodynamic studies," *Strojniški vestnik-Journal of Mechanical Engineering,* vol. 57, pp. 3-10, 2011.

[53] F. Träger, "Lasers and optics," *Section,* vol. 12, pp. 937-983, 2007.

[54] S. Antonov and V. Kotelnikov, "A review of physical principles and applications of acousto-optic deflectors on the basis paratellurite," *Phys. Astron. Int. J,* vol. 3, pp. 235-249, 2019.

[55] W. Koechner and M. Bass, *Solid-state lasers: a graduate text*: Springer Science & Business Media, 2006.

[56] P. Maak, L. Jakab, P. Richter, H. J. Eichler, and B. Liu, "Efficient acousto-optic Q switching of Er: YSGG lasers at 2.79-μm wavelength," *Applied Optics,* vol. 39, pp. 3053-3059, 2000.

[57] J. Xie, R. Guo, D. Li, C. Zhang, G. Yang, and Y. Geng, "Theoretical calculation and experimental study of acousto-optically Q-switched CO 2 laser," *Optics Express,* vol. 18, pp. 12371-12380, 2010.

[58] H. Hong, L. Huang, Q. Liu, P. Yan, and M. Gong, "Compact high-power, TEM 00 acousto-optics A3B2 show [pmg: line-break justify=" yes"/] Q-switched Nd: YVO 4 oscillator pumped at 888 nm," *Applied Optics,* vol. 51, pp. 323-327, 2012.

[59] O. Svelto and D. C. Hanna, *Principles of lasers* vol. 1: Springer, 2010.

[60] J.-P. Salvestrini, M. Abarkan, and M. Fontana, "Comparative study of nonlinear optical crystals for electro-optic Q-switching of laser resonators," *Optical Materials,* vol. 26, pp. 449-458, 2004.

[61] J. Shang, J. Sun, Q. Li, J. Yang, L. Zhang, and J. Xu, "Single-block pulse-on electro-optic Q-switch made of LiNbO 3," *Scientific Reports,* vol. 7, p. 4651, 2017.

[62] T. M. Jeong and J. Lee, "Generation of high-intensity laser pulses and their applications," *High Energy and Short Pulse Lasers,* vol. 1, 2016.

[63] T. M. Hussein and A.-K. M. Salih, "Simulation of effective area ratio effect on saturable absorber absorption activity in passive Q-switching doped fiber laser system," *SIMULATION,* vol. 54, 2022.

[64] M. Alsous, K. Almetaeb, and M. Alnezami, "Modeling of flash-pumped passively Q-switched solid state lasers," *Journal of Optics,* vol. 44, pp. 159-163, 2015.

[65] L. Li, X. Yang, L. Zhou, W. Xie, Y. Wang, Y. Shen, *et al.*, "Active/passive Q-switching operation of 2 μm Tm, Ho: YAP laser with an acousto-optical Q-switch/MoS 2 saturable absorber mirror," *Photonics Research,* vol. 6, pp. 614-619, 2018.

[66] H. Ahmad, M. Samion, A. Muhamad, A. Sharbirin, and M. F. Ismail, "Passively Q-switched thulium-doped fiber laser with silver-nanoparticle film as the saturable absorber for operation at 2.0 μm," *Laser Physics Letters,* vol. 13, p. 126201, 2016.

[67] F. B. Slimen, S. Chen, J. Lousteau, Y. Jung, N. White, S. Alam, *et al.*, "Highly efficient Tm 3+ doped germanate large mode area single mode fiber laser," *Optical Materials Express,* vol. 9, pp. 4115-4125, 2019.

[68] J. Y. Huang, H. Liang, K.-W. Su, and Y.-F. Chen, "Analytical model for the design of external-cavity passively Q-switched fiber lasers," in *Fiber Lasers V: Technology, Systems, and Applications*, 2008, pp. 426-434.

[69] Y. Shen, X. Fu, C. Yao, W. Li, Y. Wang, X. Zhao, *et al.*, "Optical crystals for 1.3 μm all-solid-state passively Q-switched laser," *Crystals,* vol. 12, p. 1060, 2022.

[70] D. Popa, Z. Sun, T. Hasan, F. Torrisi, F. Wang, and A. C. Ferrari, "Graphene Q-switched, tunable fiber laser," *Applied Physics Letters,* vol. 98, 2011.

[71] Y. Tang and J. Xu, "A random Q-switched fiber laser," *Scientific Reports,* vol. 5, p. 9338, 2015.

[72] M. Skorczakowski, J. Swiderski, W. Pichola, P. Nyga, A. Zajac, M. Maciejewska, *et al.*, "Mid-infrared Q-switched Er: YAG laser for medical applications," *Laser physics letters,* vol. 7, p. 498, 2010.

[73] M. Marconi, J. Javaloyes, S. Balle, and M. Giudici, "How lasing localized structures evolve out of passive mode locking," *Physical review letters,* vol. 112, p. 223901, 2014.

[74] R. Boyd, "Nonlinear Optics 4th edn (New York: Academic)," 2020.

[75] M. Ebrahim-Zadeh and I. T. Sorokina, *Mid-infrared coherent sources and applications*: Springer Science & Business Media, 2008.

[76] R. S. Soboh, A. H. Al-Masoodi, F. N. Erman, A. H. Al-Masoodi, B. Nizamani, H. Arof*, et al.*, "Lawsone dye material as potential saturable absorber for Q-switched erbium doped fiber laser," *Optical fiber technology,* vol. 64, p. 102537, 2021.

[77] M. M. Mafroos, H. J. Sapingi, and A. Hamzah, "Passively Q-switched erbium doped fiber laser based on graphene and carbon nanotube saturable absorbers," *Indonesian Journal of Electrical Engineering and Computer Science,* vol. 28, pp. 227-233, 2022.

[78] G. Karlsson, V. Pasiskevicius, F. Laurell, J. A. Tellefsen, B. Denker, B. I. Galagan*, et al.*, "Diode-pumped Er–Yb: glass laser passively Q switched by use of Co2+: MgAl2O4 as a saturable absorber," *Applied Optics,* vol. 39, pp. 6188-6192, 2000.

[79] Z. Yang, L. Han, J. Zhang, Y. Zhang, F. Zhang, Z. Lin*, et al.*, "Passively Q-switched laser using PtSe2 as saturable absorber at 1.3 μm," *Infrared Physics & Technology,* vol. 104, p. 103155, 2020.

[80] B. Li, Q. Chen, P. Zhang, R. Tian, L. Zhang, Q. Sai*, et al.*, "β-Ga2O3 Used as a Saturable Sbsorber to Realize Passively Q-Switched Laser Output," *Crystals,* vol. 11, p. 1501, 2021.

[81] M. Engelbrecht, F. Korte, J. Koch, D. Wandt, and C. Fallnich, "Femtosecond rapid prototyping technique for patterning of lithium niobate samples," in *Advanced Solid-State Photonics*, 2005, p. 853.

[82] W. T. Silfvast, "Fundamentals of Photonics," *University of Connecticut,* 2003.

[83] S. Chénais, F. Druon, S. Forget, F. Balembois, and P. Georges, "On thermal effects in solid-state lasers: The case of ytterbium-doped materials," *Progress in quantum electronics,* vol. 30, pp. 89-153, 2006.

[84] Y. Y. Kalisky, *The physics and engineering of solid state lasers* vol. 71: Spie Press, 2006.

[85] J. F. Becker, *Novel Laser Sources and Applications: Proceedings of a Workshop Held November 12-13, 1993, San Jose, California, USA*: SPIE Press, 1994.

[86] F. Druon, F. Balembois, and P. Georges, "New laser crystals for the generation of ultrashort pulses," *Comptes Rendus Physique,* vol. 8, pp. 153-164, 2007.

[87] S. Uemura and K. Torizuka, "Generation of 10 fs pulses from a diode-pumped Kerr-lens mode-locked Cr: LiSAF laser," *Japanese Journal of Applied Physics,* vol. 39, p. 3472, 2000.

[88] U. Demirbas, F. X. Kärtner, and M. Pergament, "Cavity-dumped nanosecond Cr: LiSAF laser in the 985–1030 nm region for versatile seeding of Yb-based amplifiers," *Applied Physics B,* vol. 128, p. 20, 2022.

[89] U. Demirbas, S. Eggert, and A. Leitenstorfer, "Compact and efficient Cr: LiSAF laser pumped by one low-cost single-spatial-mode diode," in *Laser Sources and Applications*, 2012, pp. 65-72.

[90] D. A. Biasetti, E. J. Di Liscia, and G. A. Torchia, "Optical waveguides fabricated in Cr: LiSAF by femtosecond laser micromachining," *Optical Materials,* vol. 73, pp. 25-32, 2017.

[91] M. F. Mekteplioglu, Y. Ozturk, M. Pergament, F. X. Kärtner, and U. Demirbas, "Broadly tunable (402–535 nm) intracavity frequency-doubled Cr: LiSAF laser," *Applied Physics B,* vol. 129, p. 22, 2023.

[92] W. Koechner, *Solid-state laser engineering* vol. 1: springer, 2013.

[93] N. Hodgson and H. Weber, *Laser resonators and beam propagation: fundamentals, advanced concepts and applications*: Springer, 2005.

[94] A. E. Siegman, "Unstable optical resonators for laser applications," *Proceedings of the IEEE,* vol. 53, pp. 277-287, 2005.

[95] B. E. Saleh and M. C. Teich, *Fundamentals of photonics, 2 volume set*: john Wiley & sons, 2019.

[96] A. A. Kaminskii, *Laser crystals: their physics and properties* vol. 14: Springer, 2013.

[97] P. W. Milonni and J. H. Eberly, *Laser physics*: John Wiley & Sons, 2010.

[98] V. V. Kubarev, "Babinet principle and diffraction losses in laser resonators," *Quantum electronics,* vol. 30, p. 824, 2000.

[99] M. Marconi, O. Martinez, and F. Diodati, "Short pulse generation in solid state lasers by a novel passive technique," *Optics communications,* vol. 63, pp. 211-216, 1987.

[100] R. J. Pressley, "CRC Handbook of lasers: with selected data on optical technology," *(No Title),* 1971.

[101] A. Gomes, W. Sleat, W. Sibbett, and J. Taylor, "Thirty fold pulse compression of the pulses from a Q-switched and mode locked Nd: YAG laser," *Optics communications,* vol. 57, pp. 257-262, 1986.

[102] D. Hanna, A. Kazer, and D. Shepherd, "Active mode-locking and Q-switching of a 1.54 μm Er: glass laser pumped by a 1.064 μm Nd: YAG laser," *Optics communications,* vol. 65, pp. 355-358, 1988.

[103] I. Milev, S. Dimov, S. Kurtev, O. Denchev, and I. Angelov, "Optimization of the pumping conditions for Nd: YAG lasers," *Applied optics,* vol. 29, pp. 772-776, 1990.

[104] M. W. Smillie, "Passive Q-switching of 1 micron Nd: YAG lasers for military target designator applications," 2018.

[105] I. Primsa, M. Sreenath, V. A. Kumar, and I. H. Joe, "Switching of reverse saturable absorption to saturable absorption in dye-carbon nanotube blended system under cw and q-switched laser excitation," *Journal of Molecular Liquids,* vol. 385, p. 122345, 2023.

[106] S. Saadaoui, M. A. B. Youssef, M. B. Karoui, R. Gharbi, E. Smecca, V. Strano*, et al.*, "Performance of natural-dye-sensitized solar cells by ZnO nanorod and nanowall enhanced photoelectrodes," *Beilstein journal of nanotechnology,* vol. 8, pp. 287-295, 2017.

[107] A. Lagatsky, P. Koopmann, P. Fuhrberg, G. Huber, C. Brown, and W. Sibbett, "Passively mode locked femtosecond Tm: Sc2O3 laser at 2.1 mu m," *Optics Letters,* 2012.

[108] J. Ma, G. Xie, W. Gao, P. Yuan, L. Qian, H. Yu*, et al.*, "Diode-pumped mode-locked femtosecond Tm: CLNGG disordered crystal laser," *Optics letters,* vol. 37, pp. 1376-1378, 2012.

[109] B. Yao, W. Wang, K. Yu, G. Li, and Y. Wang, "Passively mode-locked Tm, Ho: YVO 4 laser based on a semiconductor saturable absorber mirror," *Chinese Optics Letters,* vol. 10, pp. 071402-071402, 2012.

[110] A. Tyazhev, R. Soulard, T. Godin, M. Paris, G. Brasse, J. Doualan, *et al.*, "Passively mode-locked diode-pumped Tm3+: YLF laser emitting at 1.91 μm using a GaAs-based SESAM," *Laser Physics Letters,* vol. 15, p. 045807, 2018.

[111] Y. Zhao, Y. Wang, X. Zhang, X. Mateos, Z. Pan, P. Loiko, *et al.*, "87 fs mode-locked Tm, Ho: CaYAlO 4 laser at~ 2043 nm," *Optics letters,* vol. 43, pp. 915-918, 2018.

[112] K. Yang, D. Heinecke, J. Paajaste, C. Kölbl, T. Dekorsy, S. Suomalainen, *et al.*, "Mode-locking of 2 μm Tm, Ho: YAG laser with GaInAs and GaSb-based SESAMs," *Optics Express,* vol. 21, pp. 4311-4318, 2013.

[113] X. Zou, Y. Leng, Y. Li, Y. Feng, P. Zhang, Y. Hang, *et al.*, "Passively Q-switched mode-locked Tm: LLF laser with a MoS 2 saturable absorber," *Chinese Optics Letters,* vol. 13, p. 081405, 2015.

[114] C. Y. Cho, Y. F. Chen, G. Zhang, W. D. Chen, and H. C. Liang, "Exploring the self-mode locking of the 2 μm Tm: YAG laser with suppression of the self-pulsing dynamic," *Optics Letters,* vol. 42, pp. 5226-5229, 2017.

[115] W. Zhou, X. Xu, R. Xu, X. Fan, Y. Zhao, L. Li, *et al.*, "Watt-level broadly wavelength tunable mode-locked solid-state laser in the 2 μm water absorption region," *Photonics Research,* vol. 5, pp. 583-587, 2017.

[116] W.-J. Ling, T. Xia, Z. Dong, L.-F. You, Y.-Y. Zuo, K. Li, *et al.*, "1.91 μm Passively continuous-wave mode-locked Tm: LiLuF4 laser," *Optics & Laser Technology,* vol. 108, pp. 364-367, 2018.

[117] J. Ma, Z. Qin, G. Xie, L. Qian, and D. Tang, "Review of mid-infrared mode-locked laser sources in the 2.0 μm–3.5 μm spectral region," *Applied Physics Reviews,* vol. 6, 2019.

[118] Z. Zhou, X. Guan, X. Huang, B. Xu, H. Xu, Z. Cai, *et al.*, "Tm 3+-doped LuYO 3 mixed sesquioxide ceramic laser: effective 2.05 μm source operating in continuous-wave and passive Q-switching regimes," *Optics Letters,* vol. 42, pp. 3781-3784, 2017.

[119] N. Stevenson, C. Brown, J.-M. Hopkins, M. Dawson, C. Kränkel, and A. Lagatsky, "Diode-pumped femtosecond Tm 3+-doped LuScO 3 laser near 2.1 μm," *Optics Letters,* vol. 43, pp. 1287-1290, 2018.

[120] A. Gluth, Y. Wang, V. Petrov, J. Paajaste, S. Suomalainen, A. Härkönen, *et al.*, "GaSb-based SESAM mode-locked Tm: YAG ceramic laser at 2 μm," *Optics Express,* vol. 23, pp. 1361-1369, 2015.

[121] S. M. Link, A. Klenner, and U. Keller, "Dual-comb modelocked lasers: semiconductor saturable absorber mirror decouples noise stabilization," *Optics Express,* vol. 24, pp. 1889-1902, 2016.

[122] Y. Mashiko, E. Fujita, and M. Tokurakawa, "Tunable noise-like pulse generation in mode-locked Tm fiber laser with a SESAM," *Optics express,* vol. 24, pp. 26515-26520, 2016.

[123] R. Soulard, A. Tyazhev, J.-L. Doualan, A. Braud, A. Hideur, M. Laroche, *et al.*, "2.3 μm Tm 3+: YLF mode-locked laser," *Optics letters,* vol. 42, pp. 3534-3536, 2017.

[124] X. Mateos, P. Loiko, S. Lamrini, K. Scholle, P. Fuhrberg, S. Vatnik, *et al.*, "Thermo-optic effects in Ho: KY (WO 4) 2 thin-disk lasers," *Optical Materials Express,* vol. 8, pp. 684-690, 2018.

[125] G. Sobon, "Mode-locking of fiber lasers using novel two-dimensional nanomaterials: graphene and topological insulators," *Photonics Research,* vol. 3, pp. A56-A63, 2015.

[126] Q. Hu, X. Zhang, Z. Liu, P. Li, M. Li, Z. Cong, *et al.*, "High-order harmonic mode-locked Yb-doped fiber laser based on a SnSe2 saturable absorber," *Optics & Laser Technology,* vol. 119, p. 105639, 2019.

[127] Z.-C. Luo, M. Liu, A.-P. Luo, and W.-C. Xu, "Two-dimensional materials-decorated microfiber devices for pulse generation and shaping in fiber lasers," *Chinese Physics B,* vol. 27, p. 094215, 2018.

[128] K. Wu, B. Chen, X. Zhang, S. Zhang, C. Guo, C. Li, *et al.*, "High-performance mode-locked and Q-switched fiber lasers based on novel 2D materials of topological insulators, transition metal dichalcogenides and black phosphorus: review and perspective," *Optics Communications,* vol. 406, pp. 214-229, 2018.

[129] Y. Zhang, H. Wang, F. Li, X. Sun, B. Dong, X. Li, *et al.*, "The emerging ferroic orderings in two dimensions," *Science China Information Sciences,* vol. 62, pp. 1-27, 2019.

[130] K. S. Novoselov, A. K. Geim, S. V. Morozov, D.-e. Jiang, Y. Zhang, S. V. Dubonos, *et al.*, "Electric field effect in atomically thin carbon films," *science,* vol. 306, pp. 666-669, 2004.

[131] J. He, L. Tao, H. Zhang, B. Zhou, and J. Li, "Emerging 2D materials beyond graphene for ultrashort pulse generation in fiber lasers," *Nanoscale,* vol. 11, pp. 2577-2593, 2019.

[132] J. Li, Z. Zhang, L. Du, L. Miao, J. Yi, B. Huang, *et al.*, "Highly stable femtosecond pulse generation from a MXene Ti 3 C 2 T x (T= F, O, or OH) mode-locked fiber laser," *Photonics Research,* vol. 7, pp. 260-264, 2019.

[133] B. Guo, Q. l. Xiao, S. h. Wang, and H. Zhang, "2D layered materials: synthesis, nonlinear optical properties, and device applications," *Laser & Photonics Reviews,* vol. 13, p. 1800327, 2019.

[134] R. I. Woodward and E. J. Kelleher, "2D saturable absorbers for fibre lasers," *Applied Sciences,* vol. 5, pp. 1440-1456, 2015.

[135] X. Liu, Q. Guo, and J. Qiu, "Emerging low-dimensional materials for nonlinear optics and ultrafast photonics," *Advanced Materials,* vol. 29, p. 1605886, 2017.

[136] Q. Hao, C. Wang, W. Liu, X. Liu, J. Liu, and H. Zhang, "Low-dimensional saturable absorbers for ultrafast photonics in solid-state bulk lasers: status and prospects," *Nanophotonics,* vol. 9, pp. 2603-2639, 2020.

[137] Y.-K. Kuo, H.-M. Chen, and J.-Y. Chang, "Numerical study of the Cr: YSO Q-switched ruby laser," *Optical Engineering,* vol. 40, pp. 2031-2035, 2001.

[138] Y.-K. K. Lin and H.-M. Chen, "Tunable Cr: YSO Q-Switched Cr: BeAl2O4 laser: numerical study on laser performance along three principal axes of the Q switch," *Japanese Journal of Applied Physics,* vol. 39, p. 4002, 2000.

[139] A. Giese, M. Körber, K. Kostourou, D. Kopf, M. Kottcke, J. Lohbreier*, et al.*, "Passively Q-switched sub-100 ps Yb3+: YAG/Cr4+: YAG microchip laser: experimental results and numerical analysis," in *Solid State Lasers XXXII: Technology and Devices*, 2023, pp. 187-197.

[140] P. Zhao, S. Ragam, Y. J. Ding, and I. B. Zotova, "Investigation of terahertz generation from passively<? A3B2 show [pmg: line-break justify=" yes"/]?> Q-switched dual-frequency laser pulses," *Optics letters,* vol. 36, pp. 4818-4820, 2011.

[141] A. Dubois, G. Moneron, and C. Boccara, "Thermal-light full-field optical coherence tomography in the 1.2 μm wavelength region," *Optics Communications,* vol. 266, pp. 738-743, 2006.

[142] N. D. Gladkova, G. Petrova, N. Nikulin, S. Radenska-Lopovok, L. Snopova, Y. P. Chumakov*, et al.*, "In vivo optical coherence tomography imaging of

human skin: norm and pathology," *Skin Research and Technology,* vol. 6, pp. 6-16, 2000.

[143] J. M. Schmitt, A. Knuttel, M. Yadlowsky, and M. Eckhaus, "Optical-coherence tomography of a dense tissue: statistics of attenuation and backscattering," *Physics in Medicine & Biology,* vol. 39, p. 1705, 1994.

[144] M. F. Mekteplioglu, Y. Ozturk, F. X. Kärtner, and U. Demirbas, "Q-switched mode-locked Cr: LiSAF laser with broad tunability."

[145] M. Salih, "Photons Loss Simulation during Cr: YSO Passive Q-switch Ruby laser pulse Generation," *J. of Education College,* vol. 3, p. 688, 2008.

[146] D. G. Luenberger, "Linear and nonlinear," ed: Programming, Addison-Weslcy Publishing Company, 1984.

[147] S. J. Wright, "Algorithms and software for linear and nonlinear programming," in *AIChE Symposium Series*, 2000, pp. 58-69.

[148] L. Guo, G.-G. Wang, A. H. Gandomi, A. H. Alavi, and H. Duan, "A new improved krill herd algorithm for global numerical optimization," *Neurocomputing,* vol. 138, pp. 392-402, 2014.

[149] M. S. Bazaraa, J. J. Jarvis, and H. D. Sherali, *Linear programming and network flows*: John Wiley & Sons, 2011.

[150] J. K. Strayer, *Linear programming and its applications*: Springer Science & Business Media, 2012.

[151] G. Giorgi and T. H. Kjeldsen, "A historical view of nonlinear programming: Traces and emergence," in *Traces and Emergence of Nonlinear Programming*, ed: Springer, 2013, pp. 1-43.

[152] M. S. Bazaraa, H. D. Sherali, and C. M. Shetty, *Nonlinear programming: theory and algorithms*: John wiley & sons, 2006.

[153] Y. S. Sherif and B. A. Boice, "An efficient algorithm for solving the unconstrained nonlinear multivariable minimization problems," *Advances in engineering software,* vol. 17, pp. 29-37, 1993.

[154] W. Crown, N. Buyukkaramikli, P. Thokala, A. Morton, M. Y. Sir, D. A. Marshall*, et al.*, "Constrained optimization methods in health services research—an introduction: report 1 of the ISPOR optimization methods emerging good practices task force," *Value in health,* vol. 20, pp. 310-319, 2017.

[155] M. Subasi, N. Yildirim, and B. Yildiz, "An improvement on Fibonacci search method in optimization theory," *Applied mathematics and computation,* vol. 147, pp. 893-901, 2004.

[156] S. Nayak, *Fundamentals of optimization techniques with algorithms*: Academic Press, 2020.

[157] H. Das and M. B. Hasan, "A Generalized Computer Technique for Solving Unconstrained Non-Linear Programming Problems," *Dhaka University Journal of Science,* vol. 61, pp. 75-80, 2013.

[158] T. Ma, "Filtering adaptive tracking controller for multivariable nonlinear systems subject to constraints using online optimization method," *Automatica,* vol. 113, p. 108689, 2020.

[159] J. P. Mize, *Optimization techniques with FORTRAN*: McGraw-Hill, Inc., 1973.

[160] D. S. Hussein, A.-K. M. Salih, and R. Asal, "Investigation of Saturable Absorber Length Effect on Characteristics of Passive Q-Switching and Stokes with Anti-Stokes Pulses Generated in Laser System of Nd: YVO4," *University of Thi-Qar Journal of Science,* vol. 11, 2024.

[161] S. S. Rao, *Engineering optimization: theory and practice*: John Wiley & Sons, 2019.

[162] L. Ngartera and C. Diallo, "A Comparative Study of Optimization Techniques on the Rosenbrock Function," *Open Journal of Optimization,* vol. 13, pp. 51-63, 2024.

[163] M. Baudin, "Introduction to Unconstrained Optimization," 2011.

[164] L. Abualigah, A. Diabat, and R. A. Zitar, "Orthogonal learning Rosenbrock's direct rotation with the gazelle optimization algorithm for global optimization," *Mathematics,* vol. 10, p. 4509, 2022.

[165] E. Munin, A. B. Villaverde, X. Zhang, and M. Bass, "Broad-band, intensity-dependent absorption in tetravalent chromium-doped crystals," *Applied physics letters,* vol. 63, p. 1739, 1993.

الخلاصة

تهدف هذه الدراسة الى إيجاد القيم المثلى لبعض معاملات معادلات المعدل الخاصة بالليزر Cr:LiSAF العامل بالنمط المفتاحي السلبي لعامل النوعية بأستخدام Cr:YSO كمادة ماصة قابلة للاشباع.

يعتمد النموذج الرياضي المستخدم على أربع معادلات تفاضلية غير خطية من الدرجة الأولى تمثل تطور السلوك الزمني لمكونات النظام وعلى النحو التالي.

تمثل المعادلة الأولى معادلة معدل عدد فوتون التجويف (n). تمثل المعادلة الثانية معادلة معدل الكثافة العددية للتوزيع العكسي (N_g). تمثل المعادلة الثالثة معادلة معدل جزيء الامتصاص القابل للتشبع عند المستوي الأرضي (N_a). تمثل المعادلة الرابعة معادلة معدل جزيء الامتصاص القابل للتشبع عند المستوي المثارة الأول(N_{au}).
تم حلها عدديًا باستخدام طريقة رونج - كوتا – فيلبيرج لتحديد خصائص النبضة العملاقة الناتجة من الليزر.

بعد ذلك، تقنية الأمثلة تم توظيفها لتحديد قيم المعاملات التالية، مقطع امتصاص الحالة المثارة إلى مقطع امتصاص الحالة الأرضية لجزيئات الممتص القابل للتشبع (β)، معدل اضمحلال المادة الماصة القابلة للاشباع (γ_a)، معدل الخسائر الفوتونية داخل تجويف الليزر (γ_c)، بأستخدام تقنية روزنبروك المقيدة. حيث وُجد أن قيمة (β) تزداد مع زيادة عدد جزيئات Cr: YSO، لكن قيم كل من معدل استرخاء Cr: YSO (γ_a) ومعدل فقدان الفوتونات (γ_c) تنخفض مع زيادة عدد جزيئات Cr: YSO القابلة للتشبع حتى الوصول إلى قيمة معينة، وعند هذه النقطة يصبح التباين مهملاً.

كانت نسبة الخطأ المطلق بين المعلمات المحسوبة نظريا والمحسوبة عمليا هي (0.0299, 0.000009, 0.0000032)، على التوالي.

جامعة كربلاء

كلية العلوم

قسم الفيزياء

ايجاد قيم بعض معاملات معادلات المعدل لليزرات العاملة بالنمط المفتاحي السلبي باستخدام تقنية الامثلية

رسالة مقدمة إلى مجلس كلية العلوم - جامعة كربلاء وهي جزء

من نيل متطلبات درجة الماجستير في علوم الفيزياء

كتبت بواسطة

دعاء صبار سلمان

بإشراف

د. قاسم حسن عبيد

1447هـ

2025 م